REPUBLIC OF TURKEY

ADANA ALPARSLAN TÜRKEŞ SCIENCE AND TECHNOLOGY UNIVERSITY

GRADUATE SCHOOL

ELECTRICAL AND ELECTRONIC ENGINEERING DEPARTMENT

APPLICATION OF WIDE RANGE VOLTAGE INPUT DC-DC CONVERTER FOR PORTABLE HOME APPLIANCE

GÜLCAN SU ÇAPRAZ

M.Sc.

ADANA 2024

REPUBLIC OF TURKEY

ADANA ALPARSLAN TÜRKEŞ SCIENCE AND TECHNOLOGY UNIVERSITY

GRADUATE SCHOOL

ELECTRICAL - ELECTRONIC ENGINEERING DEPARTMENT

APPLICATION OF WIDE RANGE VOLTAGE INPUT DC-DC CONVERTER FOR PORTABLE HOME APPLIANCE

GÜLCAN SU ÇAPRAZ

M.Sc.

SUPERVISOR

PROF.DR. LÜTFÜ SARIBULUT

ADANA, 2024

DECLARATION OF CONFORMITY

I hereby declare that all information in this thesis has been obtained and presented in accordance with academic rules and ethical conduct. I also declare that, as required by these rules and conduct, I have fully cited and referenced all information that is not original to this work.

02/08/2024

[Signature]

Gülcan Su ÇAPRAZ

ÖZET

GENİŞ GİRİŞ VOLTAJ ARALIĞINA SAHİP DC-DC KONVERTÖRÜN TAŞINABİLİR EV ALETLERİNDE UYGULANMASI

Gülcan Su ÇAPRAZ
Yüksek Lisans, Elektrik-Elektronik Mühendisliği Anabilim Dalı

Danışman: Prof. Dr. Lütfü SARIBULUT

Ağustos 2024, 71 sayfa

Bu çalışmada geniş giriş voltaj aralığına sahip Zeta Konvertör'ün (ZK), çıkış voltajının istenilen seviyede sağlanmasındaki önemi ve uygulamalardaki performansı araştırılmıştır. Literatürde ZK'ün teorisi ve uygulaması üzerine az sayıda makale ve tez çalışmaları bulunmaktadır. Bu akademik kaynaklar arasında yapılan araştırmalarda, matematiksel denklemlerde ve ZK'ün devre eleman değerlerinin hesaplanmasında hatalara rastlanılmıştır. ZK'ün hem matematiksel teorisinin hem de uygulamasının literatürde detaylı olarak ilk kez bu tez çalışmasında sunulmuştur. MATLAB programının benzetim özelliği kullanılarak 5V–24V arasında giriş aralığına ve 12V çıkışa sahip bir ZK benzetim modeli önerilmiştir. ZK'ın çıkış voltajını istenilen seviyede sabit tutmak için Oransal-Inegral (OI) kontrol yöntemi kullanılmıştır. Elde edilen çıkış voltajı, sinüzoidal darbe-genişlik modülasyon (SDGM) yöntemi kullanılarak H-köprü evireç ile 12V alternatif gerilime dönüştürülmüş ve tek faz trafo kullanılarak gerilim seviyesi 220V değerine çıkarılmıştır. Tez kapsamında çeşitli benzetim durum çalışmaları sunulmuş ve bu çalışmaların sonuçlarında önerilen ZK'ün performansı değerlendirilmiştir.

Anahtar Kelimeler: Zeta konvertör, OI kontrolcü, SDGM, H-köprü evireç

ABSTRACT

APPLICATION OF WIDE RANGE VOLTAGE INPUT DC-DC CONVERTER FOR PORTABLE HOME APPLIANCE

Gülcan Su ÇAPRAZ
M.Sc., Department of Electrical and Electronic Engineering

Supervisor: Prof. Dr. Lütfü SARIBULUT

August 2024, 71 pages

In this study, the importance and performance of the Zeta Converter (ZK) with a wide input voltage range in maintaining the output voltage at the desired level were investigated. In the literature, there are few articles and theses on the theory and application of ZK. During the research conducted among these academic sources, errors were found in the mathematical equations and in the calculation of the ZK circuit component values. This thesis presents, for the first time in detail, both the mathematical theory and the application of ZK in the literature. A ZK simulation model with an input range of 5V–24V and a 12V output was proposed using the simulation feature of MATLAB. A Proportional-Integral (PI) control method was employed to keep the output voltage of the ZK stable at the desired level. The obtained output voltage was converted to 12V alternating voltage using the H-bridge inverter with the Sinusoidal Pulse-Width Modulation (SPWM) method, and the voltage level was increased to 220V using a single-phase transformer. Various simulation case studies were presented within the scope of the thesis, and the performance of the proposed ZK was evaluated based on the results of these studies.

Keywords: Zeta converter, PI controller,SPWM, H-bridge inverter

Dedication

I would like to dedicate my thesis to my family.

ACKNOWLEDGEMENTS

I would like to express my heartfelt thanks to my supervisor for his supervision, guidance, great support, extremely valuable advice, and encouragement throughout this thesis.

I would like to express my thanks to Research Assistant Elanur EKİCİ for her support and cooperation during my study.

I am also grateful to the members of the Electrical and Electronic Engineering Department, Adana Alparslan Türkeş Science and Technology University.

Finally, I wish to express my deepest gratitude to my husband, Baturalp ÇAPRAZ, for his endless support, encouragement, and patience. I would also like to extend my thanks to my parents for their unwavering support and encouragement.

TABLE OF CONTENTS

LIST OF FIGURES

LIST OF TABLES

LIST OF ABBREVIATIONS

AC	: Alternating Current
DC	: Direct Current
PV	: Photovoltaic
CCM	: Continuous Conduction Mode
DCM	: Discontinuous Conduction Mode
IGBT	: Insulated Gate Bipolar Transistor
MOSFET	: Metal Oxide Semiconductor Field Effect Transistor
PI	: Proportional-Integral
PID	: Proportional-Integral-Derivative
SEPIC	: Single-Ended Primary-Inductor Converter
PWM	: Pulse Width Modulation
SPWM	: Sinusoidal Pulse Width Modulation
SEPIC	: Single-Ended Primary-Inductor Converter
CUK	: Cuk Converter
BUCK	: Buck Converter
BUCK-BOOST	: Buck-Boost Converter
THD	: Total Harmonic Distortion

LIST OF SYMBOLS

AC	**:** Alternating Current
DC	**:** Direct Current
IGBT	**:** Insulated Gate Bipolar Transistor
MOSFET	**:** Metal Oxide Semiconductor Field Effect Transistor
PI	**:** Proportional-Integral
V	**:** Voltage
I	**:** Current
P	**:** Power
Z	: Impedance
L	: Inductance
C	: Capacitance
R	: Resistance
F	: Frequency
ω	**:** Angular Frequency

1. INTRODUCTION

1.1. Power Electronics Converters

Power electronics converters have attracted significant attention over time because of their essential role in various industrial applications. A power electronic device comprises a converter constructed from a matrix of power semiconductor switching elements and electronic control circuitry (Erickson et al., 2004). The following are the many types of converters: rectifiers (AC-DC converters), cyclo-converters (AC-AC converters at different frequencies), inverters (DC-AC converters), choppers (DC-DC converters), and AC power controllers (AC-AC converters at the same frequency). These power converters find widespread application in a wide range of systems, including energy storage solutions, motor drives, uninterruptible power supply, renewable energy systems (RESs), high-voltage DC transmission, power quality enhancement, and power generation and distribution. Furthermore, power converters serve as interfaces between RESs, energy storage units (ESUs), and microgrids. Employing a separate converter for each source connection increases both the cost and complexity of the system (Mohan, et al.,1995).

1.1.1. DC-DC Converters

DC-DC converters constitute fundamental components in the field of power electronics, designed to convert direct current (DC) electrical power efficiently from one voltage level to another. The primary types of DC-DC converters include buck, boost, buck-boost, and more complex configurations like the Zeta converter. Each type has unique characteristics and is selected based on specific application requirements, such as input voltage range, desired output voltage, efficiency, and system complexity (Erickson et al., 2004).

DC-DC converters are frequently employed in applications that necessitate regulated DC power, including laptop computers, communication devices, medical instruments, television receivers, battery chargers, and electric vehicles. DC-DC converters are mostly used in DC motor control, DC welding machines, feeding inverters, switched-mode power supplies, uninterruptible power supplies, power factor correction, and DC voltage sources and regulators (Rahman et al., 2011).

DC-DC converter core topologies can primarily be divided into two main categories: those that are transformerless and those that are transformer-based. Cuk converters, boost (step-up), buck-boost (step-down/step-up), and buck (step-down) are examples of transformerless topologies. On the other hand, transformer-based topologies encompass flyback, forward, and push-pull converters (Ioinovici, et al., 2013).

The buck and boost conversion modes, such as bidirectional power flow, high-frequency operation, and galvanic isolation of the isolated bidirectional DC-DC converter topology, have made it widely used. These converters are widely used in push-pull, dual-active bridge, MPC, isolated Cuk, and single-ended primary-inductor converter (SEPIC)/Zeta topologies, among other power electronics applications. Achieving variable voltage regulation and high-efficiency power conversion in high-performance bidirectional power converters poses several design and implementation problems. In recent years, the integration of bidirectional DC-DC converter topologies into DC microgrids has emerged as a prominent research area (Jozwik, et al., 1989).

1.1.1.1 Zeta Converter

The Zeta converter is a unique type of DC-DC converter that offers significant advantages over traditional converters. Its ability to maintain the intended output voltage regardless of whether the input voltage is higher or lower than the output (Woranetsuttikul, et al., 2014). Additionally, the Zeta converter does not invert the polarity of the output voltage, which simplifies the design of power systems and ensures compatibility with various loads. The flexibility and robustness of the Zeta converter make it an ideal choice for power applications requiring stable and reliable voltage regulation (Niculescu et al., 2008).

1.2. Sine Pulse Width Modulation (SPWM) Inverters

Sine Pulse Width Modulation (SPWM) inverters are used to convert DC output of the Zeta converter to AC voltage. SPWM is a widely used technique in power electronics for generating high-quality AC signals with low harmonic distortion. The method involves modulating the width of the pulses in a sinusoidal manner, which effectively reduces the harmonic content and results in a cleaner AC output. This is crucial for applications where electrical noise and efficiency are of paramount importance, such as in renewable energy systems and uninterruptible power supplies (UPS) (B. Ismail, et al., 2006).

1.3. Proportional-Integral (PI) Control Method

By using the proportional-integral (PI) control technique, the output voltage of the Zeta converter is maintained at the proper level. The PI control strategy is favoured for its simplicity and effectiveness in addressing both the instantaneous value and the accumulated value over time of the error in a feedback loop. By continuously adjusting the control input based on the error signal, the PI controller ensures that the output voltage remains stable and within the desired range. This enhances the overall stability and dynamic performance of the system, making it more resilient to disturbances and variations in input voltage (K. J. Åström., et al., 2004).

1.4. Objectives of the Thesis

1.4.1 Design and Analyse the Zeta Converter

- Regardless of the input voltage's variation, a thorough design for the Zeta converter will be created to ensure a steady output voltage.

- A detailed analysis of the Zeta converter's performance characteristics, including efficiency, voltage regulation, and output stability, will be conducted.

1.4.2. Implement the Proportional-Integral (PI) Control Method

- A Proportional-Integral (PI) control algorithm specifically tailored for the Zeta converter will be formulated to ensure precise and stable output voltage regulation.

- Tests and assessments will be conducted to determine how well the PI control mechanism maintains the intended output voltage under various operating situations.

1.4.3. To Implement Proportional-Integral (PI) Control Method

- To convert the DC output of the Zeta converter into a single-phase AC voltage, an SPWM inverter will be created.

- It will be ensured that the SPWM technique effectively reduces harmonic distortion, resulting in a clean AC output with low electrical noise.

1.4.4. To Develop and Validate Simulation Models

- Detailed simulation models of the Zeta converter, PI control algorithm, and SPWM inverter will be developed by using MATLAB/Simulink.

- The simulation models will be used to optimize system parameters for improved performance and efficiency.

- Simulation results will be compared with theoretical projections to verify the effectiveness of the proposed system design.

1.5. Outline of the Thesis

The structure of the thesis is organized as follows:

- Chapter 1 introduces the Zeta converter, Single Phase SPWM H-Bridge Inverter, and the PI Control Method. General information about power electronic converters and DC-DC converters is also provided.

- Chapter 2 offers a detailed explanation of the Zeta converter and Single Phase SPWM H-Bridge Inverter, along with a thorough comparison found in the literature.

- Chapter 3 discusses the operating modes of the Zeta converter and Single Phase SPWM H-Bridge Inverter.

- Chapter 4 focuses on control methods, providing an in-depth description.

- Chapter 5 presents and discusses the simulation results of six different case studies.

- Chapter 6 highlights the significant findings and main contributions of the study. Finally, the thesis concludes with relevant references and the author's biographical information.

2. LITERATURE REVIEW

2.1. Review of Zeta Converter

Circuits known as DC-DC converters change the voltage level of a DC signal at their inputs based on the occupancy rate of the control signal sent to the switching element and transmitted to the converter's output (Erickson et al., 2004). Power electronics' main branch, DC-DC conversion, is advancing quickly. Converters are frequently utilised in applications for DC motor drives and regulated switching mode DC power supplies. Because they are used so frequently, several topologies are continually being researched (Mohan et al., 1995). The zeta converter is a unique type of converter that has been developed to sustain a constant output voltage from an input voltage that varies above and below the intended output level. (Khaleghi et al.,2014). In numerous residential and industrial applications, zeta is frequently employed.

The Zeta converter is operating in Continuous Conduction Mode (CCM) dynamic modelling and control demonstrated (Vuthchhay et al., 2008a). Its operating in Continuous Conduction Mode (CCM) investigated and mathematical expressions for current and voltage parameters have been obtained (Martins et al., 1993). In order to verify the mathematical expressions, simulation study and laboratory prototype were analysed and reported. This study is valuable because it was the first applied study.

After the Zeta converter became known, in some studies, the Zeta converter was compared with other voltage step-down/boost converters (Cuk, Buck-Boost) (Niculescu et al., 2006). Analysing the polarity of the input and output voltages revealed the Zeta converter's superiority over the Cuk converter. In the Cuk converter, the input and output signals have opposite polarity, whereas in the Zeta converter, the input and output waveforms have the same polarity. This makes the Zeta converter more suitable for use in distributed power systems (Jozwik et al., 1989).

Performance of SEPIC and Zeta converters is contrasted. Their effectiveness and output signals were discussed for this purpose, and the outcomes were validated on a prototype circuit. When examined in terms of voltage fluctuation on the output signal, it has been shown that the Zeta converter performs much better, especially at low switch transmission angles. Thanks to the LC filter at its output, the Zeta converter has lower output ripple than the SEPIC converter (Woranetsuttikul et al., 2014).

The Zeta converter allows for easier correction and shows less output-voltage ripple. Smaller output capacitors can be used to efficiently meet the need for load voltage ripple thanks to the Zeta converter's steady output current. It is evident that output voltage ripple and peak overshoot under transient situations are minimized, even with fluctuations in load. Additionally, it keeps the output voltage constant under different load scenarios (Babu et al., 2015).

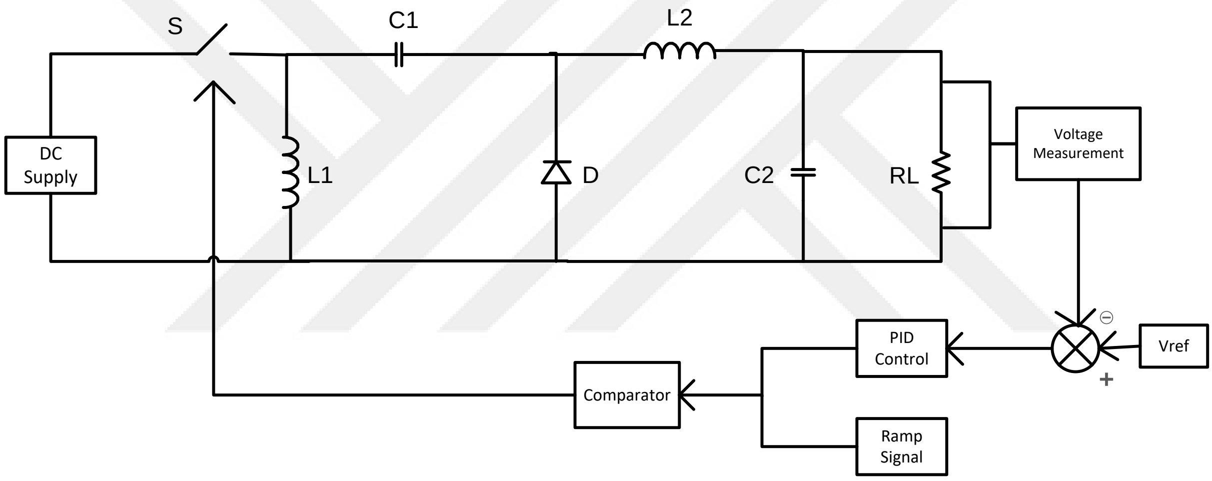

Figure 2.1. Circuit of zeta converter (Babu et al., 2015)

In studies, the classifications of Zeta converters were made according to control mode (voltage-current), transmission type (continuous-discontinuous) and power circuits were obtained. These can be listed as follows.

The primary transfer functions of the Pulse Width Modulation (PWM) Zeta converter operating in discontinuous conduction mode (DCM) demonstrate frequency characteristics akin to those observed in the converter operating under continuous conduction mode (CCM). The comprehensive AC model of the PWM Zeta converter operating in Discontinuous Conduction Mode (DCM) provides a detailed analysis of its small-signal, low-frequency dynamic characteristics (Niculescu et al., 2008). In another study for DCM study, a model was created to show that the Zeta converter had low total harmonic distortion, taking into account the dynamics at low frequencies. This model was obtained in accordance with the isolated circuit for voltage mode control and this model was validated on the prototype circuit. (Lin et al., 2005). Small signal analysis was generalized for the Zeta converter operating in DCM. Voltage mode control was made for low frequencies and the analysis was tested with experimental work through a simple control algorithm. (Viero et al., 2011).

To establish a small-signal linear dynamic model for the converter along with its multiple transfer functions, the State-Space Averaging (SSA) method was employed (Vuthchhay et al, 2008b). This was the first and most detailed study in the literature. The control-to-output transfer function was inferred, and the PWM feedback controller was designed to regulate the output voltage. The results showed that both at steady state and during a step load shift, the PWM feedback converter operated satisfactorily. (Vuthchhay et al., 2010).

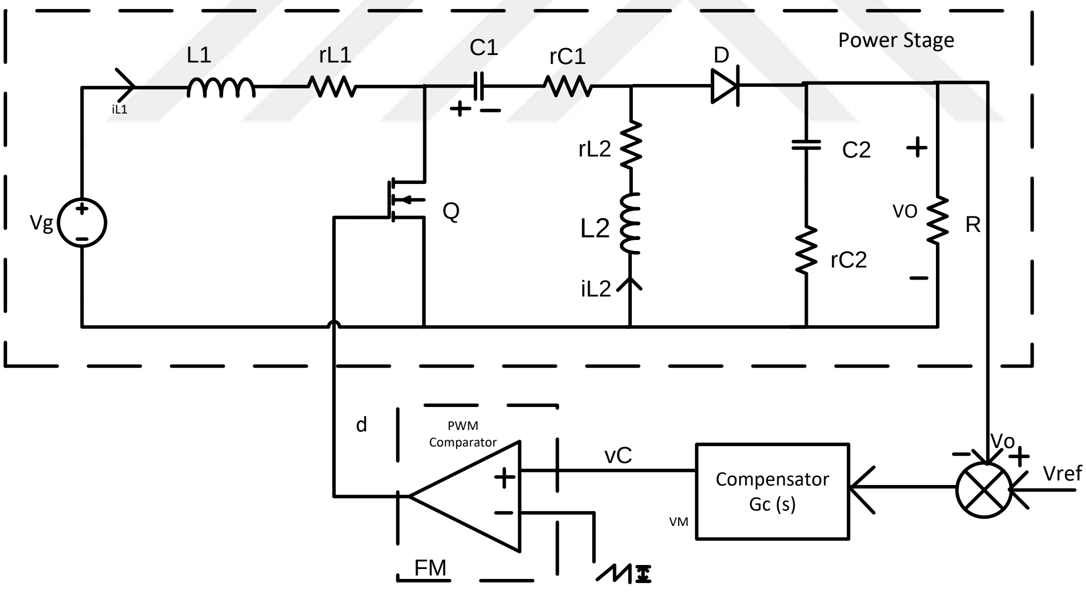

Figure 2.2. Zeta converter with PWM feedback control (Vuthchhay et al., 2010).

Small signal analysis was performed by using the models obtained by the State-Space Averaging (SSA) method. Small signal analysis was performed in CCM for the peak module current controlled, non-isolated Zeta converter topology. PWM switch was used in the analysis and the transfer function from control to output was obtained in symbolic form (Yılmaz et al., 2017).

The voltage mode control model was obtained by using the SSA method to simulate and analyse the Zeta transducer operating in CCM. Proportional-integral-derivative (PID) controller performance was investigated for steady-state behaviour of proposed method (Babu et al., 2015).

Using state-space approach and the Leverrier algorithm, the small-signal transfer function for the duty cycle to output voltage of the DC-DC Zeta converter was derived. Then, to design a PI controller that met a specific phase margin and desired crossover frequency, stability equations were applied to this transfer function. In addition, the controller works effectively when the input voltage and load resistance changed. (Garg et al., 2015). Another method for controlling the output voltage of a DC to DC Zeta converter was the Fractional Degree Proportional Integral Derivative (FOPID) controller. Compared with PID controller, FOPID controller employs fewer on-off switching actions. The results demonstrated that a FOPID controller can enhance the zeta converter's start-up response and reduce transient disturbances and switching-related losses. The Artificial Bee Colony (ABC) Algorithm, which might be used with any model of boost converter, was the basis of the suggested technique for FOPID controller parameter optimisation. This technique enables the use of a few hardware and software techniques for the effective construction of the controllers in robotics and industrial applications (Durgadevi et al., 2018).

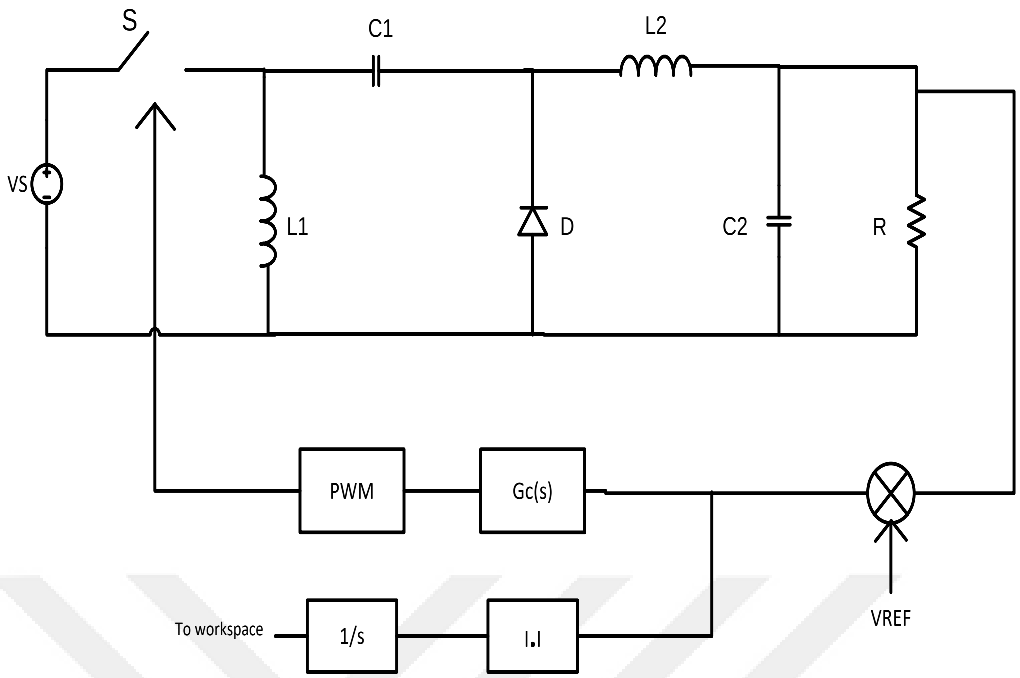

Figure 2.3. DC –DC zeta converter with FOPID controller (Durgadevi et al., 2018).

2.2. Review of Single Phase SPWM H-Bridge Inverter

Converters are a category of power electronic circuits utilized across various domains, capable of managing and controlling power flow within a system. Primarily, converters facilitate the conversion between direct current (DC) and alternating current (AC), thereby enabling the connection of systems with differing operating voltages and/or frequencies. Inverters represent a specific type of converter, specifically designed to convert DC to AC. (Rahman et al., 2011).

The output voltage of inverters varies based on the circuit topology, resulting in two, three, and multilevel waveforms. There are three distinct topologies for multilevel inverters: diode-clamped multilevel inverter (DC-MLI), flying-capacitor multilevel inverter (FC-MLI), and cascaded H-bridge multilevel inverters (CHB-MLI). (Wu B et al., 2016). Multilevel converters were initially introduced in 1975. (Baker R..H. et al., 1975). The series connection of two-level voltage source converters produced a staircase output waveform. Following that, numerous alternative multilevel converter topologies have been introduced. In 1981, a bridge converter circuit was proposed. (Baker R..H. et al., 1981). In that particular year, a neutral-point clamped multilevel inverter topology was introduced. (Nabae A. et al., 1981). In 1996, various multilevel inverter topologies were introduced, and prospective application areas were scrutinized. (Jih-Sheng Lai. et al., 1996). The subsequent year saw the introduction of a cascaded multilevel inverter topology incorporating distinct DC sources. (Peng F. Z. et al., 1997). In that year, a multilevel converter topology was introduced, incorporating AC to DC conversion capability. Moreover, in 2001, an adjustable power supply based on multilevel converter technology was introduced. (Aiello M. F. et al., 2001).

Multilevel inverters represent distinct categories within multilevel converters. A multilevel inverter's principal goal is to use independent DC sources on the input side to produce an output waveform with a high-power rating that is staircase shaped. These separate DC sources can be capacitors, renewable energy sources, or batteries. (Rodriguez J. et al., 2002).

Multilevel inverters provide numerous advantages over conventional two-level inverters. Reduced voltage stress (dv/dt), lower total harmonic distortion (THD), less electromagnetic interference (EMI), smaller output filter, and higher fundamental output are a few of these advantages. Another is the capacity to achieve higher output voltage at lower switching frequencies. (Alkhazragi. et al., 2017).

In power electronics, a commonly used method for digitizing electricity is called sinusoidal pulse width modulation (SPWM). This technique allows a series of voltage pulses to be generated through the on and off states of power switches. In single-phase and three-phase inverters, SPWM approach is utilized to attain a sinusoidal output waveform. (B. Ismail, et al., 2006).

SPWM stands out as the most widely employed method in motor control and inverter applications. Both unipolar and bipolar SPWM voltage modulation types are chosen due to their inherent advantage of effectively doubling the switching frequency of the inverter voltage. This characteristic results in a smaller, more cost-effective, and easier-to-implement output filter. Traditionally, to produce this signal, the frequency of a sinusoidal wave, which serves as the carrier signal, is compared to that of a triangular wave, which serves as the target frequency. (L. Bowtell, et al., 2007).

Constant amplitude pulses with different duty cycles for every period characterize SPWM approaches. To manage and reduce the harmonic content of the inverter output voltage, pulse width modulation was carried out. (P.Zope, et al., 2012). The utilization of the SPWM method enhances efficiency and minimizes total harmonic distortion in the output voltage. It was observed that the output current and voltage waveforms of both single-phase and three-phase inverters exhibited the desired output voltage with the expected amplitude and frequency. The unfiltered voltage and IGBT/Diode current waveforms demonstrated a similar nature. These conditions were met when utilizing an RL load. (Nagarajan, et al., 2016).

The power transistors in the H-bridge of the unipolar-switching inverter are controlled by the microcontroller, which saves and carries out instructions to create pulses with the proper waveform. This method of switching was selected for its potential to reduce switching losses, minimize Electromagnetic Interference (EMI), decrease filter sizes, and enhance Total Harmonic Distortion (THD) performance. The microcontroller stores instructions, executes them, and generates waveform pulses to precisely control the power transistors in the H-bridge of the unipolar-switching inverter. This method of switching was selected for its potential to reduce switching losses, minimize EMI, decrease filter sizes, and enhance THD performance. (Albu. Et al., 2023).

The cascaded H-bridges inverter is designed and implemented with three, five, and seven levels, employing both SPWM and Modified Sinusoidal Pulse Width Modulation (MSPWM) techniques. The results, in terms of THD before and after filtering, are compared. The MSPWM technique demonstrates a lower THD compared to SPWM. An increase in the number of levels results in reduced THD for both methods. (Alkhazragi. et al., 2017). Multilevel inverters employing the MSPWM control technique find practical utility in industrial settings, particularly in applications requiring adjustable speed drives. (Antar. et al., 2018).

A single-phase variant of a 7-level cascaded H-bridge multilevel inverter (CHB-MLI) featuring IGBTs (Insulated Gate Bipolar Transistor) as switching devices has been demonstrated. The inverter was controlled via SPWM. A range of switching frequencies, modulation indices, and load circumstances were used to analyse the inverter losses. Switching losses were responsible for most of the losses since SPWM, a high-frequency method, was used. (B. Alamri. et al., 2015).

A real-time calculation method has been introduced for CHB multilevel inverters modulated by PSC-PWM (Phase-Shifted Carrier Pulse-Width Modulation). By strategically choosing between the conventional sampling mode and the newly suggested mode, it effectively alleviated the duty cycle constraints resulting from computational delays. The modulating waveform's real-time calculation seamlessly transitions between these two sampling modes. The dynamic performance of the control loop was seen a significant enhancement with the implementation of this real-time calculation method. Additionally, the proposed approach proves effective in suppressing the impact of grid voltage distortion on the line current. (J. Ma. et al., 2020).

3. MODELLING OF CONVERTER AND INVERTER

3.1. Zeta Converter

In the proposed ZK, a constant DC output will be obtained despite the variable DC input voltage and converted to AC voltage with the inverter to be designed.

The DC-DC converter, which was introduced by Jóźwik and Kazimierczuk in the late 1980s under the name "dual of the SEPIC converter" (Jozwik, et al., 1989), is called the Zeta DA-DA converter in the literature. The designation of the name 'Zeta' for this new converter topology was attributed to it being the sixth DC-DC converter introduced in the literature. The converter was named 'Zeta' due to its association with the sixth letter of the Greek alphabet, Zeta. (Ioinovici, et al.,2013).

The proposed Zeta Converter, which consists of maintain the constant output voltage. Like the Cuk and SEPIC converters, the Zeta converter consists of a pair of active and passive switches, two inductors, and two capacitors. The switching element is situated within the buck converter section. It is evident that the gate or source of the MOSFET intended for switching purposes is not grounded in its referencing. This shows that an external driver circuit will be needed to drive the circuit. Zeta converter is obtained by starting from the cascade of buck-boost and buck converters. Since there is no need to use some switching elements in the cascade structure, Zeta topology was obtained by removing them. The circuit illustrates a current output characteristic in response to a voltage-fed input. In this way, Zeta type converters can transmit their output by increasing or decreasing the voltage at the input. This makes the Zeta converter useful for applications such as battery charging.

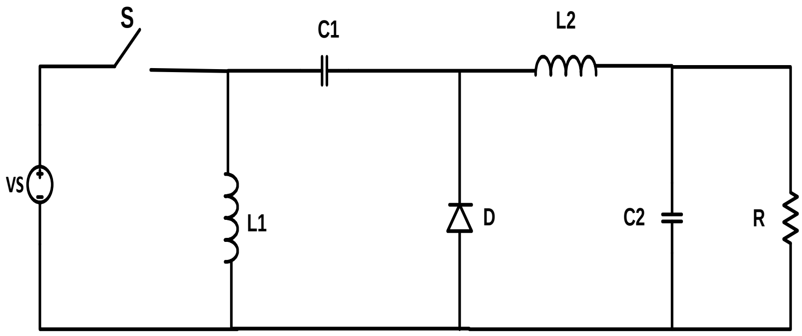

Figure 3.1. Basic structure of zeta converter

Analogous to other converter topologies, the analysis of the Continuous Conduction Mode (CCM) characteristic is contingent upon the operational state of the switch within the Zeta converter, determining whether it is in a conducting or non-conducting mode. The two portions of the converter circuit are depicted in Figures 3.2 and 3.3. In Figure 3.2, the situation when the S_1 switch is in transmission is taken into account. Figure 3.3 shows the operating logic of the circuit when the switch is open.

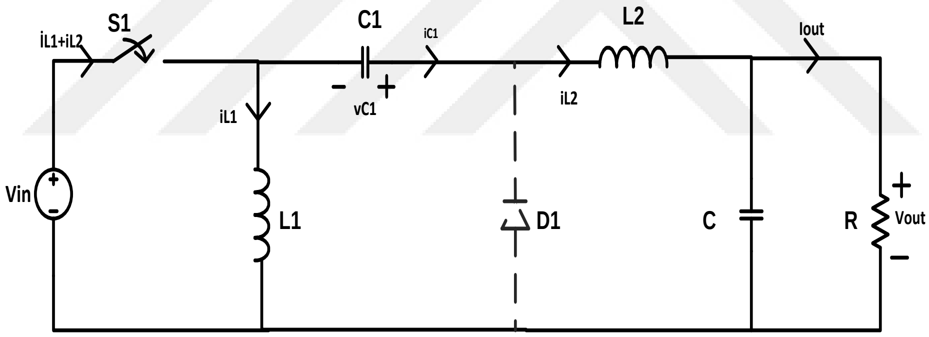

Figure 3.2. Zeta Converter when switch is ON

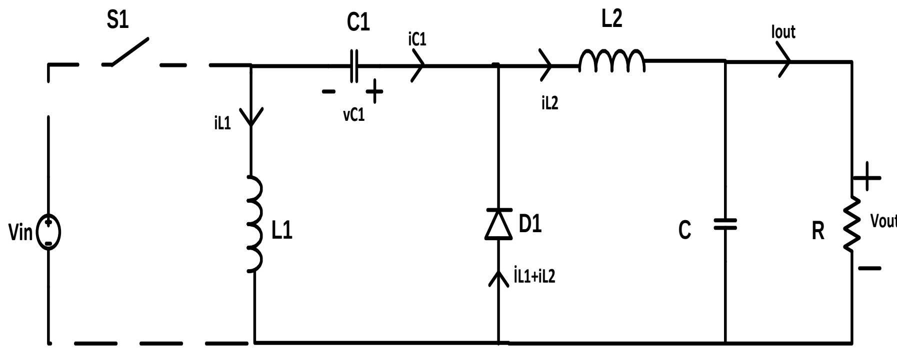

Figure 3.3. Zeta Converter when switch is OFF

3.1.1 Continuous Conduction Mode (CCM) of Zeta Converter

When the switch is switched on, the energy of the source at the input of the circuit is transferred to the circuit and the L_1 inductor is charged. It is certain that the inductor will charge, but since nothing can be said about the polarity of the C_1 capacity, for a more comprehensive understanding of the circuit, it is advisable to assess the system starting from the point at which the switch is opened (Figure 3.3). During the time the switch is open, the previously loaded L_1 inductor will begin to lose energy. Since the current will continue to flow in the same direction, it will prefer to flow through the diode (D_1), which is the path that will offer the least resistance. Therefore, the diode will be in conduction during the time the switch is open. The current will continue through the L_1 inductor and D_1 diode and complete the cycle. It is clearly seen that the circuit element that completes this cycle is C_1. It will not be possible for both reactive elements (L_1 and C_1) to lose energy at the same time on this cycle. For this reason, C_1 is charged during this time period by feeding on the magnetic energy stored on L_1. Thus, the polarity of the C_1 capacity is obtained as in Figure 3.3. Of course, the current direction shown in Figure 3.3 for the C_1 capacity is opposite, but since the current direction was not known initially, the directions were chosen randomly. Additionally, the direction of the current may differ from topology to topology (Yılmaz et al., 2017).

Therefore, if the direction of the current is chosen opposite, the equation becomes as follows. $i_{c_1}(t) = -i_{L_1}(t)$. Since the polarity of the C_1 capacity is determined, when the switch is in conduction, the D1 diode is disabled due to the polarities of the C_1 and L_1 elements. In this case, the load accumulated in the capacity C_1 flows through L_2 and this equality is obtained: $i_{C_1}(t) = i_{L_2}(t)$. As a result, the energy accumulated on the supply source and C_1 capacity is transferred to the L_2 inductor. In this way, the load connected in parallel to the output capacity C takes energy (Yılmaz et al., 2017). This part of the circuit is a typical chase operation. The sum of the currents feeding the inductors also passes through the switch. The expression of the current on switch S_1 is obtained as $i_{S_1}(t) = i_{L_1}(t) + i_{L_2}(t)$. During the period when the switch is open, the L_2 inductor also begins to lose energy. Since the D_1 diode is in conduction, the current flowing through the L_2 inductor also passes through the diode. As a result, current from both inductors flows through the diode. The diode current is like this: $i_{D_1}(t) = i_{L_1}(t) + i_{L_2}(t)$.

3.1.1.2 Continuous-State Analysis for Continuous Conduction Mode Operation of the Zeta-Type Converter

Utilizing Kirchhoff's Voltage Law (KVL), equations can be derived for the time intervals during which the switch is closed and open in Figures 3.2 and 3.3. Furthermore, for the L_1 inductor, equations corresponding to $v_{L_1}(t) = v_{in}$ can be formulated for the time interval during which the switch is in the conducting state, and equations corresponding to $v_{L_1}(t) = -v_{C_1}(t)$ can be derived for the time interval during which the switch is open. Moreover, for the L_2 inductor, equations corresponding to $v_{L_2}(t) = V_{in} + v_{C_1}(t) - V_{out}$ be derived for the period during which the switch is in the conducting state, and equations corresponding to $v_{L_2}(t) = -V_{out}$ can be formulated for the period during which the switch is open. Proceeding from here, equations (3.1) and (3.2) are derived.

$$V_{in} = v_{L_1}(t); \quad V_{in} = -v_{c_1}(t) + v_{L_2}(t) + V_{out}, \qquad 0 \le t < DT_s \tag{3.1}$$

$$v_{L_1}(t) + v_{C_1}(t) = 0; \quad v_{L_2}(t) + V_{out} = 0, \qquad DT_S \le t < T_S \tag{3.2}$$

In equations (3.1) and (3.2), $v_{L_1}(t)$, $v_{L_2}(t)$, and $v_{C_1}(t)$ represent the time-dependent variation of voltage across inductors L_1, L_2, and capacitor C_1, respectively. V_{in} and V_{out} denote the input and output voltages, respectively. The switching period and pulse width of switch S_1 are denoted by T_S and D, respectively. The inductors charge during one of the time intervals when the switch is in the conducting state and discharge during the other when it is in non-conductive state. Thus, when it is analysed over a single period, the following equations can be formulated for the continuous state of the inductors.

$$\int_0^{T_s} v_{L_1}(t)dt = 0 \text{ and } \int_0^{T_s} v_{L_2}(t)dt = 0 \tag{3.3}$$

The expression for the average voltage across capacitor C_1 can be calculated by examining the voltage variation over one period, as indicated by the following equation.

$$V_{C_1} = \frac{1}{T_s}\int_0^{T_s} v_{C_1}(t)dt \tag{3.4}$$

The equations obtained in (3.1) and (3.2) result in the expressions in (3.5) and (3.6) when substituted for the equations in (3.3) and (3.4).

$$\int_0^{DT_s} V_{in}dt - \int_{DT_s}^{T_s} v_{C_1}(t)\,dt = V_{in}DT_s - V_{C_1}(1-D)T_s = 0 \tag{3.5}$$

$$\int_0^{DT_s} (V_{in} + v_{C_1}(t) - V_{out})dt - \int_{DT_s}^{T_s} V_{out}dt = (V_{in} + V_{C_1} - V_{out})DT_s - V_{out}(1-D)T_s = 0 \tag{3.6}$$

When equations (3.5) and (3.6) are solved, (3.7) and (3.8) are obtained, respectively. This result indicates that in the ideal case, the average voltage across capacitor C_1 is equal to the output voltage.

$$V_{C_1} = \frac{D}{1-D}V_{in} \tag{3.7}$$

$$V_{out} = \frac{D}{1-D}V_{in} \tag{3.8}$$

The obtained result leads to equations $v_{L_1}(t) = v_{in}$ and $v_{L_2}(t) = V_{in} + V_{C_1} - V_{out} = V_{in}$ for the time interval when the switch is in the conducting state, and equations $v_{L_1}(t) = -V_{C_1} = -V_{out}$ and $v_{L_2}(t) = -V_{out}$ for the time interval when the switch is in non-conductive state.

According to these obtained results, the relationship between the input and output voltages, represented by equation (3.8), is the same as that for the SEPIC converter. Additionally, similar to the SEPIC converter, the Zeta converter is also a non-inverting power supply. By employing the aforementioned equations, it is possible to compute the currents in the inductors. Equation (3.9) serves as the expression for the current in inductor L_1 during the switch's conduction interval, while equation (3.10) provides the current expression for inductor L_1 during the switch's off interval.

$$V_{in} = v_{L_1}(t) = L_1 \frac{di_{L_1}}{dt} \qquad 0 \le t < DT_s$$

$$i_{L_1}(t) = I_{L1_{\min}} + \frac{V_{in}}{L_1} t \quad \rightarrow \quad I_{L1_{\max}} = I_{L1_{\min}} + \frac{V_{in}}{L_1} DT_S \tag{3.9}$$

$$-V_{out} = v_{L_1}(t) = L_1 \frac{di_{L_1}}{dt} \qquad DT_S \le t < T_S$$

$$i_{L_1}(t) = I_{L1_{\max}} - \frac{V_{out}}{L_1}(t - DT_S) \rightarrow I_{L1_{\min}} = I_{L1_{\max}} - \frac{V_{out}}{L_1}(T_S - DT_S) \tag{3.10}$$

By utilizing equations (3.9) and (3.10), it is also possible to calculate the magnitude of the current ripple on the L_1 output inductor.

$$\Delta I_{L1} = I_{L1_{\max}} - I_{L1_{\min}} = \frac{V_{in}}{L_1} DT_S = \frac{V_{in} D}{L_1 f_s} = \frac{V_{out}(1-D)}{L_1 f_s} \tag{3.11}$$

Starting from equation (3.11), the necessary equation for calculating the value of the selected inductor can be obtained as (3.12).

$$L_1 = \frac{V_{in} D}{\Delta L_1 f_s} = \frac{V_{out}(1-D)}{\Delta L_1 f_s} \tag{3.12}$$

Starting from equations (3.9), (3.10), and (3.11), the expression for the average current on the L_1 inductor (input inductor current) can also be derived.

$$I_{L1} = I_{L1_{\min}} + \frac{\Delta I_{L1}}{2} = I_{L1_{\min}} + \frac{V_{in} D}{2 L_1 f_s} = I_{L1_{\min}} + \frac{V_{out}(1-D)}{2 L_1 f_s} \tag{3.13}$$

Similar to the input inductor, for the time period when the switch is in the on state, equation (3.14) is obtained, while for the time period when it is in non-conductive state, equation (3.15) can be derived as the expression for the L_2 inductor current.

$$V_{in} = v_{L_2}(t) = L_2 \frac{di_{L2}}{dt} \qquad 0 \le t < DT_s$$

$$i_{L_2}(t) = I_{L2_{\min}} + \frac{V_{in}}{L_2} t \rightarrow I_{L2_{\max}} = I_{L2_{\min}} + \frac{V_{in}}{L_2} DT_S \tag{3.14}$$

$$-V_{out} = v_{L_2}(t) = L_2 \frac{di_{L2}}{dt} \qquad DT_S \le t < T_S$$

$$i_{L_2}(t) = I_{L2_{\max}} - \frac{V_{out}}{L_2}(t - DT_S) \rightarrow I_{L2_{\min}} = I_{L2_{\max}} - \frac{V_{out}}{L_2}(1-D)T_S \tag{3.15}$$

Starting from equations (3.14) and (3.15), it is possible to compute the magnitude of the current ripple on the L_2 output inductor.

$$\Delta I_{L2} = I_{L2_{\max}} - I_{L2_{\min}} = \frac{V_{in}}{L_2} DT_S = \frac{V_{in} D}{L_2 f_s} = \frac{V_{out}(1-D)}{L_2 f_s} \tag{3.16}$$

By starting from equation (3.16), the necessary equation (3.17) is obtained for the calculation of the inductor value to be selected.

$$L_2 = \frac{V_{in}D}{\Delta L_2 f_s} = \frac{V_{out}(1-D)}{\Delta L_2 f_s} \tag{3.17}$$

By utilizing equations (3.14), (3.15), and (2.16), the expression for the average current on the L_2 inductor (output inductor current) can also be derived.

$$I_{L2} = I_{L2_{\min}} + \frac{\Delta I_{L2}}{2} = I_{L2_{\min}} + \frac{V_{in}D}{2L_2 f_s} = I_{L2_{\min}} + \frac{V_{out}(1-D)}{2L_2 f_s} \tag{3.18}$$

The expression for the current across the S_1 switch during its conducting interval is derived by considering the summation of inductor currents. The current value of switch S_1 reaches its maximum at the instant of DT_S. In instances where the S_1 switch is in a non-conductive state, the cumulative inductor currents delineate the current traversing diode D_1. D_1 diode current reaches its maximum value at the onset of the non-conductive time interval, denoted as DT_S (when the switch is in the off state). More detailed information on this subject has been presented in previous studies within the literature. (Yılmaz et al., 2017).

When examining the representations in Figures 3.2 and 3.3, it is observed that the current flowing through capacitor C1 is equal to current $i_{L_2}(t)$ when the switch is in the conducting state and equal to current $-i_{L_1}(t)$ when the switch is in non-conducting state. Hence, starting from here, the current expressions for capacitor C_1 can be derived as in equations (3.19) and (3.20).

$$i_{C_1}(t) = i_{L_2}(t) = I_{L2_{\min}} + \frac{V_{in}}{L_2}t \qquad 0 \le t < DT_s \tag{3.19}$$

$$i_{C_1}(t) = -i_{L_1}(t) = -\left[I_{L1_{\max}} - \frac{V_{out}}{L_1}(t - DT_S) \right] = -\left[I_{L1_{\min}} + \frac{V_{in}}{L_1}DT_S - \frac{V_{out}}{L_1}(t - DT_S) \right]$$

$$i_{C_1}(t) = -I_{L1_{\min}} - \frac{V_{in}}{L_1}DT_S + \frac{D}{1-D}\frac{V_{in}}{L_1}(t - DT_S) \qquad DT_S \le t < T_S$$

$$i_{C_1}(t) = -I_{L1_{\min}} - \frac{V_{in}}{L_1}\left[DT_S - \frac{D(t-DT_S)}{1-D}\right] \qquad DT_S \le t < T_S \tag{3.20}$$

For any capacitance on a continuously operating DC-DC converter, the net current over one switching period must be equal to zero. (Erickson, et al., 2004). This is called the current-second balance principle or the charge balance principle for capacitance. Therefore, proceeding from this point, the current expression for the capacitance C_1 is formulated as follows.

$$\frac{1}{T_S}\int_0^{T_S} i_{C_1}(t)\,dt = 0$$

When substituting the current values for the conducting and off state intervals of the switch into the capacitance C, equation (3.21) is obtained.

$$\frac{1}{T_S}\int_0^{T_S} i_{C_1}(t)\,dt = \frac{1}{T_S}\left[\int_0^{DT_S} i_{L_2}(t)\,dt - \int_{DT_S}^{T_S} i_{L_1}(t)\,dt\right] = 0 \rightarrow \int_0^{DT_S} i_{L_2}(t)\,dt = \int_{DT_S}^{T_S} i_{L_1}(t)\,dt$$

$$\int_0^{DT_S}\left(I_{L2_{\min}} + \frac{V_{in}}{L_2}t\right)dt = \int_{DT_S}^{T_S}\left(I_{L1_{\min}} + \frac{V_{in}}{L_1}\left[DT_S - \frac{D(t-DT_S)}{1-D}\right]\right)dt \ \text{v}$$

$$I_{L2_{\min}} DT_S + \frac{V_{in}(DT_S)^2}{2L_2} = I_{L1_{\min}}(1-D)T_S + \frac{V_{in}(1-D)DT_S{}^2}{2L_1} \tag{3.21}$$

The average inductor current expressions derived in equations (3.13) and (3.18) are utilized to update equation (3.21), resulting in equation (3.22). This equation provides the ratio of the average currents in the inductors of the Zeta DC-DC converter.

$$I_{L2}DT_S = I_{L1}\left(1-D\right)T_S \rightarrow I_{L2}D = I_{L1}\left(1-D\right) \rightarrow \frac{I_{L_1}}{I_{L_2}} = \frac{D}{\left(1-D\right)} \tag{3.22}$$

As a result, under the assumption of 100% efficiency, the relationship between input and output currents, as well as average inductor voltages, is obtained as in equation (3.23).

$$\frac{V_{out}}{V_{in}} = \frac{I_{in}}{I_{out}} = \frac{I_{L_1}}{I_{L_2}} = \frac{D}{\left(1-D\right)} \tag{3.23}$$

The average current on the output capacitance C, being zero according to the charge balance principle, results in the output average current for the Zeta converter being equal to the average currents in inductors I_{out} and L_2, denoted as I_{L2}. In accordance with equation (3.23), it is demonstrated that the input average current (I_{in}) is equal to the average current in the input inductor (I_{L1}). The results obtained from equations (3.13) and (3.18) allow expressing the maximum and minimum inductor current values in terms of the output current and output voltage.

If the effective current is to be calculated, the approximation of equation (3.24) is obtained. Due to the relatively small current fluctuations on inductors L_1 and L_2, they have been neglected, and the effective current on capacitance C_1 has been directly calculated based on the average current values. In order to derive the final form of equation (3.24), the insights gained from equation (3.23) have been employed.

$$I_{C1_{ef}} = \sqrt{\frac{1}{T_S}\left\{\int_0^{T_S} i_{C_1}{}^2\left(t\right)dt\right\}} = \sqrt{\frac{1}{T_S}\left\{\int_0^{DT_S} i_{L_2}{}^2\left(t\right)dt + \int_{DT_S}^{T_S}\left(-i_{L_1}\left(t\right)\right)^2 dt\right\}}$$

$$I_{C1_{ef}} \approx \sqrt{\frac{1}{T_S}\left\{\int_{0}^{DT_S} I_{L_2}{}^2 dt + \int_{DT_S}^{T_S} I_{L_1}{}^2 dt\right\}} = I_{out}\sqrt{\frac{D}{(1-D)}} \quad (3.24)$$

While analyzing the voltage fluctuation across capacitance C_1, it is essential to take equation $\Delta V_{C_1} = V_{C1_{max}} - V_{C1_{min}}$ into account. In this calculation, it is possible to consider either the time interval when the switch is in the conducting state or the time interval when it is in the non-conducting state. If the time interval when the switch is in the non-conducting state is considered, it is observed that the capacitor is being charged by inductor L_1 during this time. If, for ease of analysis during this time interval, the inductor current is assumed to be constant and equal to the effective current, the voltage fluctuation for capacitance C_1 can be obtained as in equation (3.25), illuminated by the relationship (3.23).

$$\Delta V_{C_1} = \frac{1}{C_1}\int_{DT_S}^{T_S} I_{L_1} dt = \frac{1}{C_1}\int_{DT_S}^{T_S} I_{in} dt = \frac{I_{in}(1-D)T_S}{C_1} = \frac{I_{out}(1-D)T_S V_{out}}{V_{in}C_1} = \frac{DV_{out}}{RC_1 f_s} \quad (3.25)$$

If similar analyses are desired for the output capacitance C, the assumption can be made that all AC fluctuation components of inductor L_2 current pass through the output capacitance C. Based on this, the current through capacitance C can be obtained by directly subtracting the average value of the same current from inductor L2 current. By utilizing equation (3.23), the final form of equation (3.26) is attained.

$$i_C(t) = i_{L_2}(t) - I_{L_2} = i_{L_2}(t) - I_{out} \quad (3.26)$$

It has been previously emphasized that the Zeta DC-DC converter is obtained through the cascaded connection of buck and buck-boost converters. As mentioned here, it is noteworthy that the output stage is essentially identical to a buck-type DC-DC converter. From this point onwards, utilizing the equations found in the literature as buck converter relationships (Ioinovici, et al., 2013), the equations for output voltage ripple and effective value of output capacitance current are directly appended below.

$$\Delta V_{out} = \frac{(1-D)V_{out}}{8L_2Cf_s^{\ 2}} + r_C \frac{(1-D)V_{out}}{L_2 f_s} \tag{3.27}$$

The term r_C shown in equation (3.27) represents the internal resistance of capacitance C. Neglecting this resistance, the first part of the equation provides an expression for the output voltage ripple. Equation (3.28) provides the effective value of the output capacitance current. Equations (3.27) and (3.28) reach their maximum values when the duty cycle D is at its lowest. Considering these maximum values, the selection of capacitance C should be made.

$$I_{C_{ef}} = \frac{(1-D)V_{out}}{\sqrt{12}L_2 f_s} \tag{3.28}$$

3.1.2 State Space Model

The approach known as state-space averaging (SSA) is commonly used in switching converter modelling. The development of the state-space averaged model involves the creation of equations for the rates of change of the capacitor voltage and inductor current.

A system's state-variable description is articulated as follows.

$$\dot{X} = Ax + BU \tag{3.29}$$

$$V_O = Cx + EU \tag{3.30}$$

A, an nxn matrix; B, an nxm matrix; C, an mxn matrix; and D, reserved for representing the duty cycle ratio. In the case of a system employing a two-switch topology, the state equations can be formulated when the switch is closed.

$$\dot{X} = A_1x + B_1U \tag{3.31}$$

$$V_O = C_1x + E_1U \tag{3.32}$$

When switch is open mode;

$$\dot{X} = A_2 x + B_2 U \tag{3.33}$$

$$V_O = C_2 x + E_2 U \tag{3.34}$$

When the switch is closed for a duration of DT and open for (1-D)T, the equations' weighted average is as follows.

$$\dot{X} = \left[A_1 D + A_2 (1-D)\right] x + \left[B_1 D + B_2 \left(1-D\right)\right] U \tag{3.35}$$

$$V_O = \left[C_1 D + C_2 \left(1-D\right)\right] x + \left[E_1 D + E_2 \left(1-D\right)\right] U \tag{3.36}$$

Let us consider the variables.

$$x_1 = i_{L1} \tag{3.37}$$

$$x_2 = i_{L2} \tag{3.38}$$

$$x_3 = V_{C1} \tag{3.39}$$

$$x_4 = V_{C2} \tag{3.40}$$

$$U = V_{in} \tag{3.41}$$

$$\frac{di_{L1}}{dt} = \frac{Vin}{L_1} \tag{3.42}$$

$$\frac{di_{L2}}{dt} = \frac{Vin}{L_2} + \frac{V_{C1}}{L_2} - \frac{V_{C2}}{L_2} \tag{3.43}$$

$$\frac{dV_{C1}}{dt} = -\frac{i_{L2}}{C_1} \tag{3.44}$$

$$\frac{dV_{C2}}{dt} = \frac{i_{L2}}{C_2} - \frac{V_{C2}}{R_L C_2} \tag{3.45}$$

$$\frac{di_{L1}}{dt} = -\frac{V_{C1}}{L_1} \tag{3.46}$$

$$\frac{di_{L2}}{dt} = -\frac{V_{C2}}{L_2} \tag{3.47}$$

$$\frac{dV_{C1}}{dt} = \frac{i_{L1}}{C_1} \tag{3.48}$$

$$\frac{dV_{C2}}{dt} = \frac{i_{L2}}{C_2} - \frac{V_{C2}}{R_L C_2} \tag{3.49}$$

The 'on' state's state-space equation is derived from equations (3.42), (3.43), (3.44), and (3.45) as follows.

$$\begin{bmatrix} \dot{X}_1 \\ \dot{X}_2 \\ \dot{X}_3 \\ \dot{X}_4 \end{bmatrix} = \begin{bmatrix} 0 & 0 & 0 & 0 \\ 0 & 0 & \frac{1}{L_2} & -\frac{1}{L_2} \\ 0 & -\frac{1}{C_1} & 0 & 0 \\ 0 & \frac{1}{C_2} & 0 & -\frac{1}{C_2 R_L} \end{bmatrix} \begin{bmatrix} x_1 \\ x_2 \\ x_3 \\ x_4 \end{bmatrix} + \begin{bmatrix} \frac{1}{L_1} \\ \frac{1}{L_2} \\ 0 \\ 0 \end{bmatrix} [U] \tag{3.50}$$

The 'off' state's state-space equation is derived from equations (3.46), (3.47), (3.48), and (3.49) as follows.

$$\begin{bmatrix} \dot{X}_1 \\ \dot{X}_2 \\ \dot{X}_3 \\ \dot{X}_4 \end{bmatrix} = \begin{bmatrix} 0 & 0 & -\frac{1}{L_1} & 0 \\ 0 & 0 & 0 & -\frac{1}{L_2} \\ \frac{1}{C_1} & 0 & 0 & 0 \\ 0 & \frac{1}{C_2} & 0 & -\frac{1}{C_2 R_L} \end{bmatrix} \begin{bmatrix} x_1 \\ x_2 \\ x_3 \\ x_4 \end{bmatrix} \tag{3.51}$$

The state space equivalent equation of the system is derived using the equations characterizing the on-state and off-state.

$$\begin{bmatrix} \dot{X}_1 \\ \dot{X}_2 \\ \dot{X}_3 \\ \dot{X}_4 \end{bmatrix} = \begin{bmatrix} 0 & 0 & -\frac{(1-D)}{L_1} & 0 \\ 0 & 0 & \frac{D}{L_2} & -\frac{1}{L_2} \\ \frac{(1-D)}{C_1} & -\frac{D}{C_1} & 0 & 0 \\ 0 & \frac{1}{C_2} & 0 & -\frac{1}{C_2 R_L} \end{bmatrix} \begin{bmatrix} x_1 \\ x_2 \\ x_3 \\ x_4 \end{bmatrix} + \begin{bmatrix} \frac{D}{L_1} \\ \frac{D}{L_2} \\ 0 \\ 0 \end{bmatrix} [U] \tag{3.52}$$

$$C = \begin{bmatrix} 0 & 0 & 0 & 1 \end{bmatrix} \begin{bmatrix} x_1 \\ x_2 \\ x_3 \\ x_4 \end{bmatrix} \tag{3.53}$$

$$E = [0] \tag{3.54}$$

MATLAB coding can be used to obtain the transfer function once the values of A, B, C, and E have been determined. All Matlab code of transfer function parameters were given at Appendix function.

3.2. Single Phase SPWM H-Bridge Inverter

3.2.1. Inverters

Inverters, in the structure of inverters are devices that utilize advanced semiconductor switches such as MOSFET or IGBT (Insulated Gate Bipolar Transistor) at their outputs, transforming DC electrical energy at their inputs into AC electrical energy. (Ankit, et al., 2018). Power MOSFETs are employed for power levels below 10kW and high frequency switching operations (20-800 kHz). On the other hand, IGBTs are used for medium to high power applications exceeding 100 kW. However, achieving extremely high-frequency switching using IGBTs is impractical, as their switching frequency is limited to 20 kHz. (Jana, J., et al., 2016). Inverters provide a constant voltage and frequency despite varying load conditions. The voltage at the output of the inverter is an adjustable alternative with controllable amplitude and frequency, but it is not sinusoidal. The desired output is a pure sinusoidal alternative voltage. However, obtaining a pure sinusoidal voltage at the inverter output is not possible by simply changing the voltage waveform (B. Ismail, et al., 2006). The obtained voltage at the output is a waveform with the frequency of the output and sinusoidal voltages with certain amplitudes at harmonics and multiples of this frequency.

In other words, the inverter output voltage is a waveform with harmonics, containing harmonic components in addition to the pure sinusoidal fundamental voltage. If the goal is to achieve a pure sinusoidal waveform at the output, in the design, it is inevitable to eliminate or negligibly consider these harmonics that occur (B. Alamri. et al., 2015).

Inverters can be categorized based on the characteristics of the power supply or the number of phases. In practice, inverters are divided into two groups according to the characteristics of the power supply: current-fed and voltage-fed inverters. The choice between current-fed and voltage-fed inverters depends on the characteristics of the load. Current-fed inverters control the AC waveform, being supplied from the DC-link coil. Similarly, voltage-fed inverters control the AC voltage waveform while being supplied from a DC-link capacitor. When comparing these two types of inverters, it has been proven that the design of voltage-fed inverters is more efficient, providing higher reliability and faster dynamic response. (Molina, M. G., et al., 2016).

Inverters are classified into two groups based on the number of phases, either single-phase or three-phase. Single-phase inverters are further categorized as half-bridge or full-bridge inverters. Among these, half-bridge inverters have a simple circuit structure consisting of two switches, as illustrated in Figure 3.4. However, these types of inverters have a low input voltage and high voltage across the switches. Additionally, half-bridge inverters exhibit significant output voltage or current harmonics, leading to increased costs for filtering. (Liao, Z., et al., 2019).

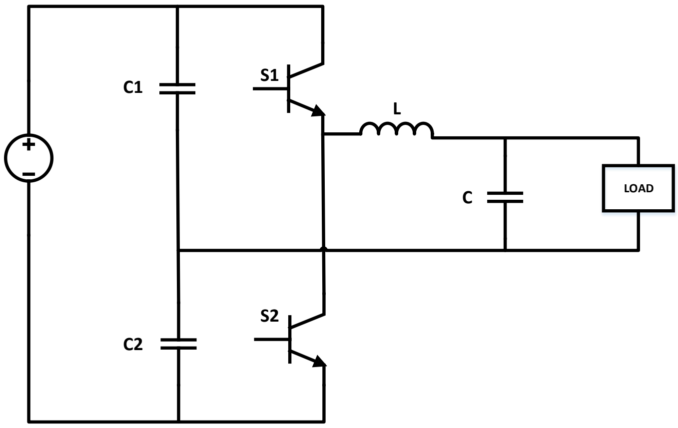

Figure 3.4. The circuit structure of a single-phase half-bridge inverter

As seen in Figure 3.5, four solid-state switches make up a single-phase full bridge inverter. The midpoints of the left and right legs of the bridge circuit, respectively, are where the two terminals of the load or network are connected.

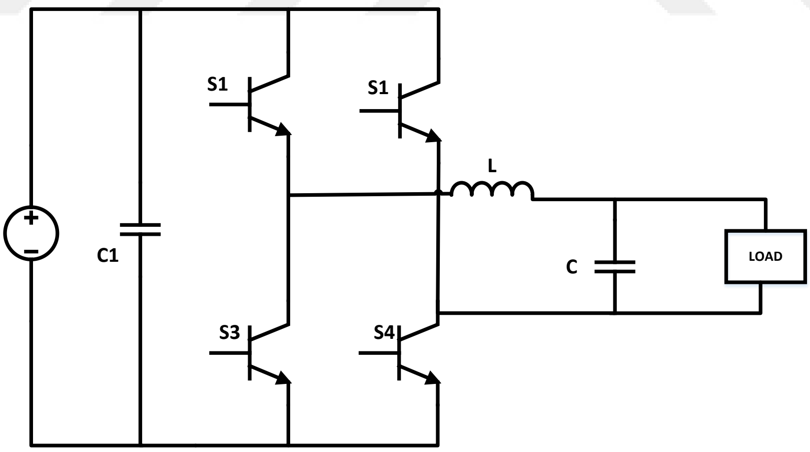

Figure 3.5. The circuit structure of a single-phase full-bridge inverter

Single-phase full bridge inverters have different output voltages depending on the conduction/cutting status of the switches.

Three-phase inverters are employed for medium to high-power applications (>5 kW), such as the grid integration of various renewable energy sources and diverse industrial applications (Jana, J., et al., 2016).

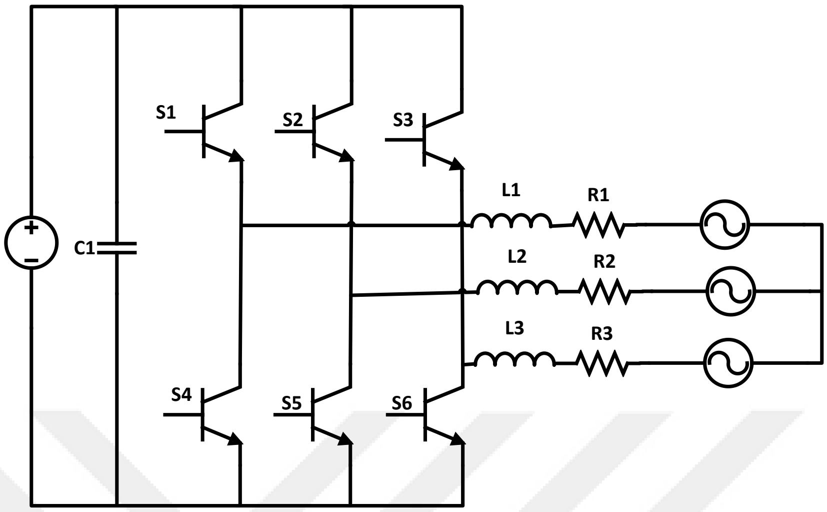

Figure 3.6. The circuit structure of a three-phase grid-connected inverter

3.2.2. Sinusoidal Pulse Width Modulation

PWM is a widely employed technique in the design of electronic power circuits. It enables designers to achieve output voltages of higher quality, which can be easily filtered. Among the various PWM techniques SPWM is a common technique known for generating a sinusoidal signal and minimizing harmonic distortions. (Albu, et al., 2021).

The SPWM technique involves the utilization of two waveforms: a reference waveform and a carrier waveform. The reference waveform is sinusoidal and operates at a fundamental frequency, whereas the carrier waveform is triangular with a higher frequency. The inverter's switching frequency is determined by the carrier waveform's frequency, with higher carrier frequencies leading to higher switching frequencies. The reference waveform's frequency sets the inverter's output frequency, achieved by comparing it with the carrier waveform. The modulation index controls the fundamental frequency component of the output voltage. (Arab, M., et al., 2014).

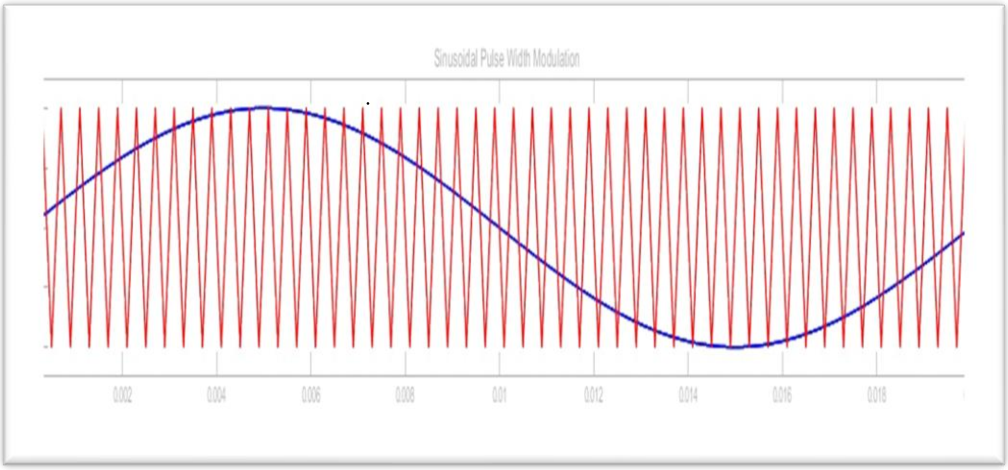

Figure 3.7. Sinusoidal pulse width modulation (Red ones is carrier signals, blue ones is reference signal) (Sinusoidal signal frequency is 2*π*50 hz)

High-quality output voltage is achieved by employing multiple modulations, particularly with a sine reference wave, known as SPWM technique. Frequency modulation and amplitude modulation rate are two crucial factors that define the SPWM technique. (Barge., et al., 2013).

3.2.3. Frequency Modulation Ratio

The frequency modulation ratio is the ratio of the carrier signal frequency to the reference signal frequency. Certain harmonics, exceeding the fundamental frequency, can be effectively eliminated with a low-pass filter due to their higher frequencies. Elevating the carrier frequency can result in an increase in the frequencies at which harmonics manifest. (Mazumder., et al., 2017).

$$mf = \frac{fcarrier}{freference} = \frac{ftriangular}{fsine} > 1 \qquad (3.55)$$

Modulation is termed synchronous if *mf* ∈ N (natural numbers) and asynchronous if *mf* ∈ R (real numbers). In the case of synchronous modulation, the presence of higher harmonics depends on *mf*. (Namboodiri., et al., 2015).

3.2.4. Amplitude Modulation Ratio:

The amplitude modulation ratio is the ratio of the reference signal amplitude to the carrier signal amplitude. (Mazumder., et al., 2017).

$$ma = \frac{Vm{,}reference}{Vm{,}carrier} = \frac{Vm{,}sine\ or\ Vm{,}control}{Vm{,}triangular} \tag{3.56}$$

Vm,reference and *Vm,carrier* represent the peak values of the modulating waveform and the carrier waveform, respectively. The modulation index is governed by the peak amplitude, and consequently, it regulates the root mean square (rms) output voltage of the inverter. (Jung., et al., 2009).

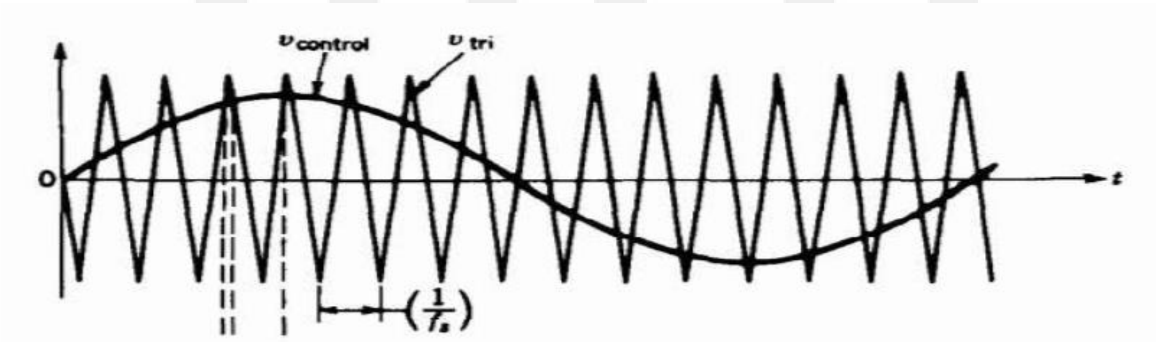

Figure 3.8. Vm, control and Vm,triangular signals (P.Zope, et al., 2012).

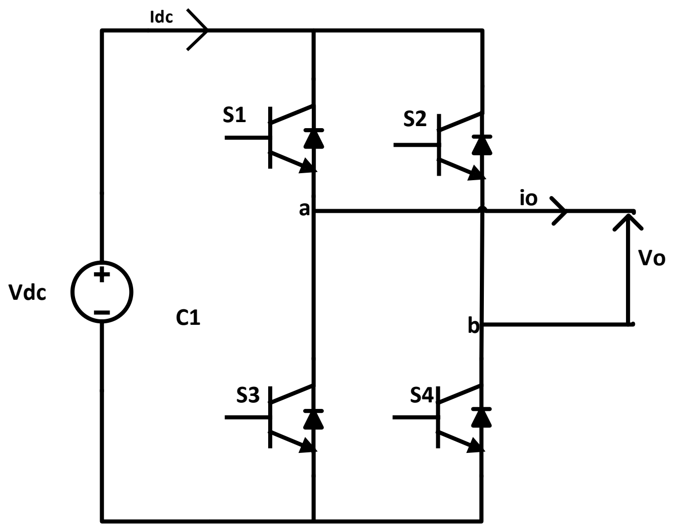

Figure 3.9. Topology of H-bridge inverter

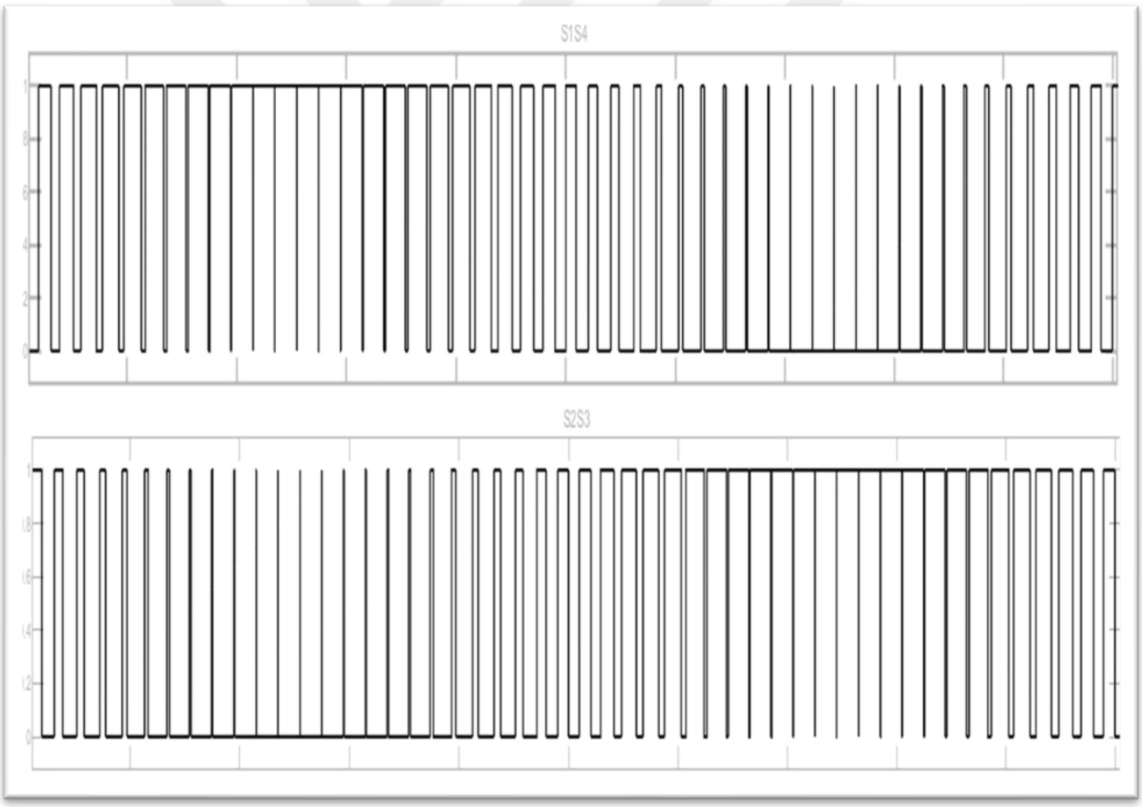

Figure 3.10. Gating pulses for S1 and S4, gating pulses for S2 and S3

There are two different PWM techniques for full-bridge inverters: unipolar switching PWM and bipolar switching PWM.

Bipolar PWM produces a ±Vdc two-level voltage when a single reference AC signal at the fundamental frequency is compared to a high-frequency carrier signal over a switching period. Both positive and negative pulses can be simultaneously generated from the circuit. The upper and lower switches in the same inverter leg function complementarily, with one switch being on when the other is off. In the bipolar switching scheme, the carrier and modulating signals are compared. The inverter switches are activated when the reference signal is greater than the carrier signal, and vice versa. (J. Soomro., et al., 2016). The switching states for bipolar PWM are detailed in Table 3.1.

Table 3.1: Bipolar PWM switching states and outputs

Output Voltage	Switch States		Power Path	
	S_1	S_2	$i_{0>0}$	$i_{0<0}$
Vdc	ON	OFF	S_1C_1	D_1C_1
-Vdc	OFF	ON	D_2C_2	S_2C_2

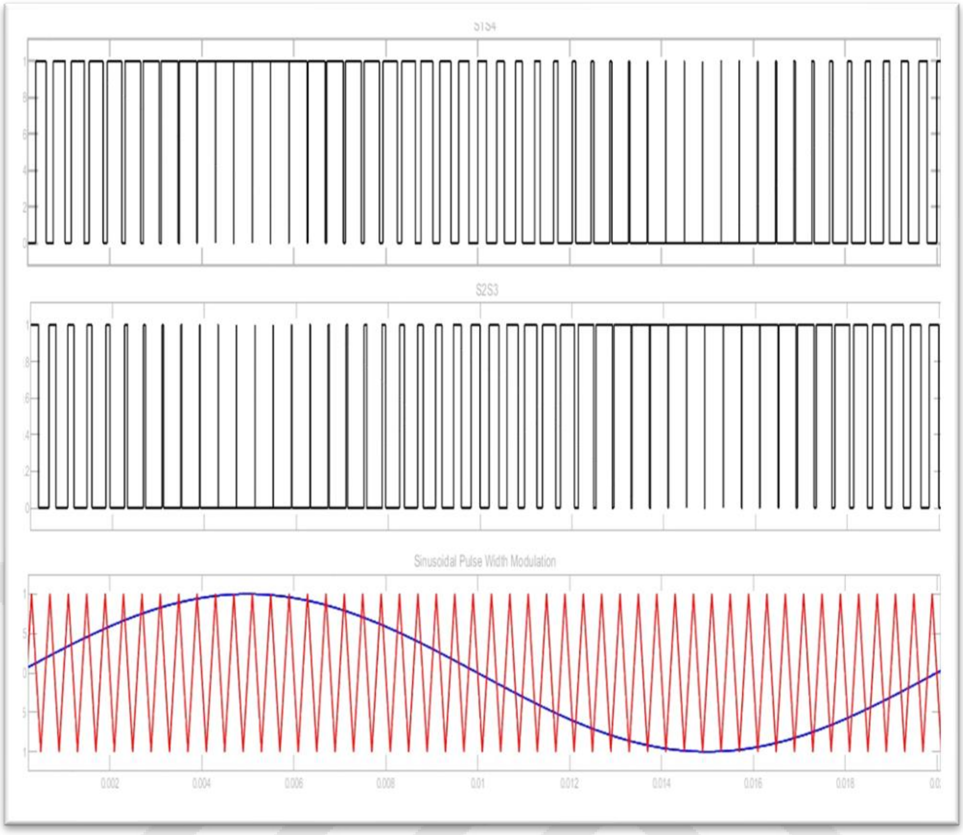

Figure 3.11: Bipolar PWM

The system incorporates two sinusoidal signals, denoted as (Vm, reference), which have the same frequency and magnitude as depicted in Figure 3.11 but are phase-shifted by 180 degrees. These sinusoidal signals, one positive and one negative, are compared with a triangular carrier signal (Vm, triangular). When these signals are utilized, the upper and lower switches operate complementarily (J. Soomro., et al., 2016). The output voltage of the inverter alternates between zero and either positive or negative voltage at the fundamental frequency. When compared to the bipolar switching method, the unipolar voltage switching strategy reduces the output voltage's harmonic content (E. H. E. Aboadla., et al., 2016).

Table 3.2: Unipolar PWM switching states and outputs

Output Voltage	Switch States				Power Path	
	S_1	S_2	S_3	S_4	$i_{0>0}$	$i_{0<0}$
Vdc	ON	OFF	OFF	ON	S_1S_4	D_1D_4
0	ON	ON	OFF	OFF	S_1D_2	S_2D_1
	OFF	OFF	ON	ON	S_4D_3	S_3D_4
-Vdc	OFF	ON	ON	OFF	D_2D_3	S_2S_3

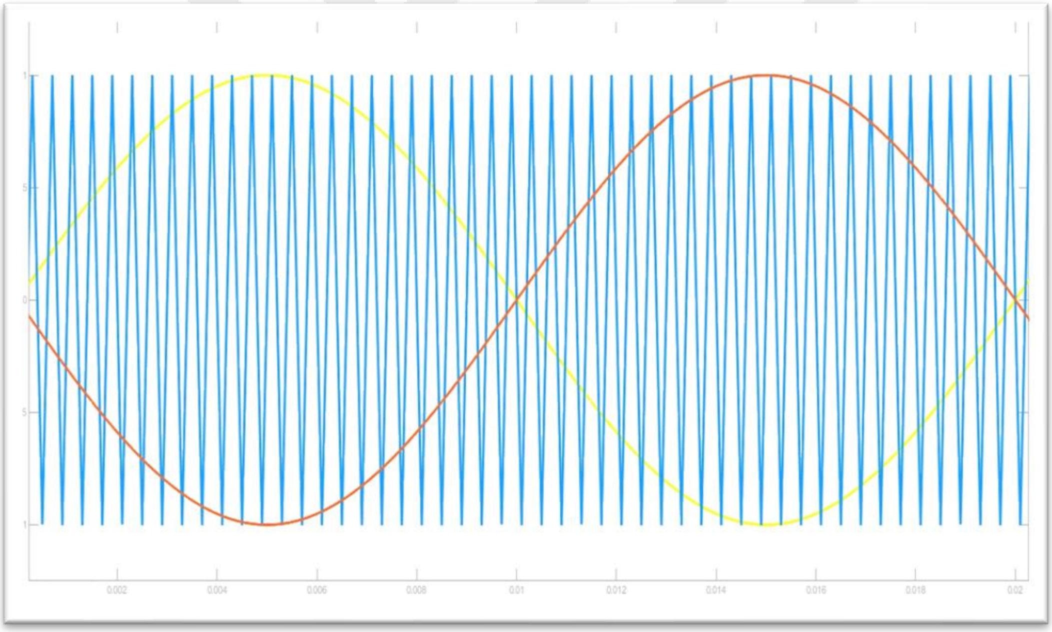

Figure 3.12: Bipolar PWM switching states (Yellow ones is reference1 signals, red ones is reference2 signal and blue ones is carrier signals)

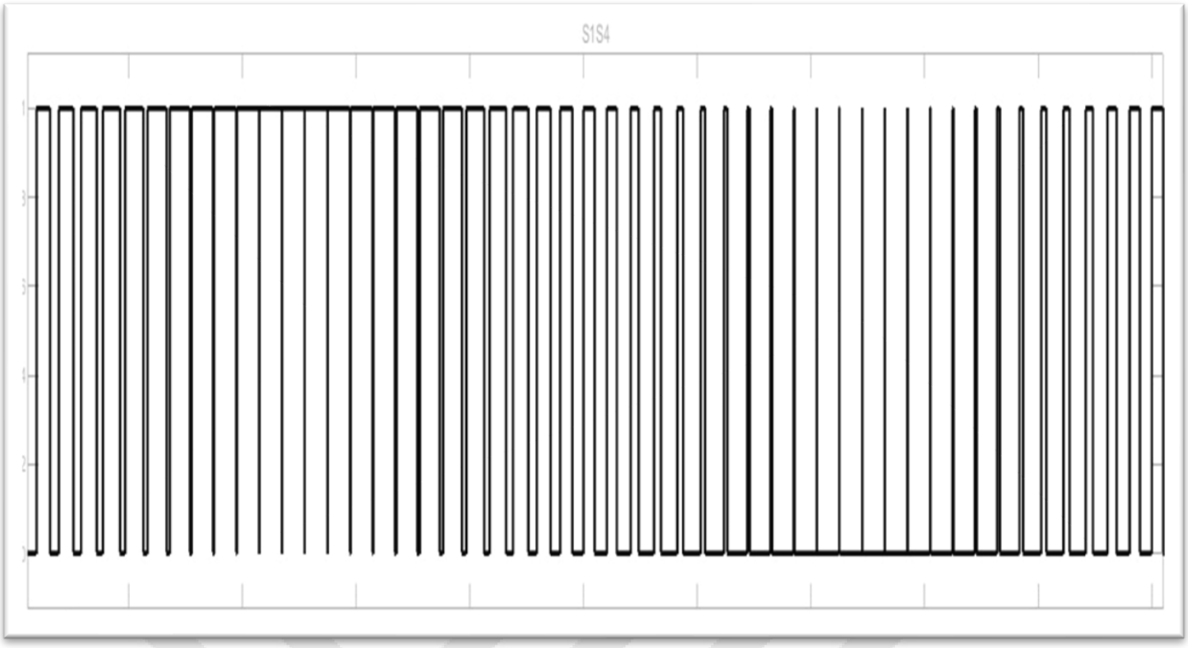

Figure 3.13: Bipolar PWM gating pulses for S1 and S4

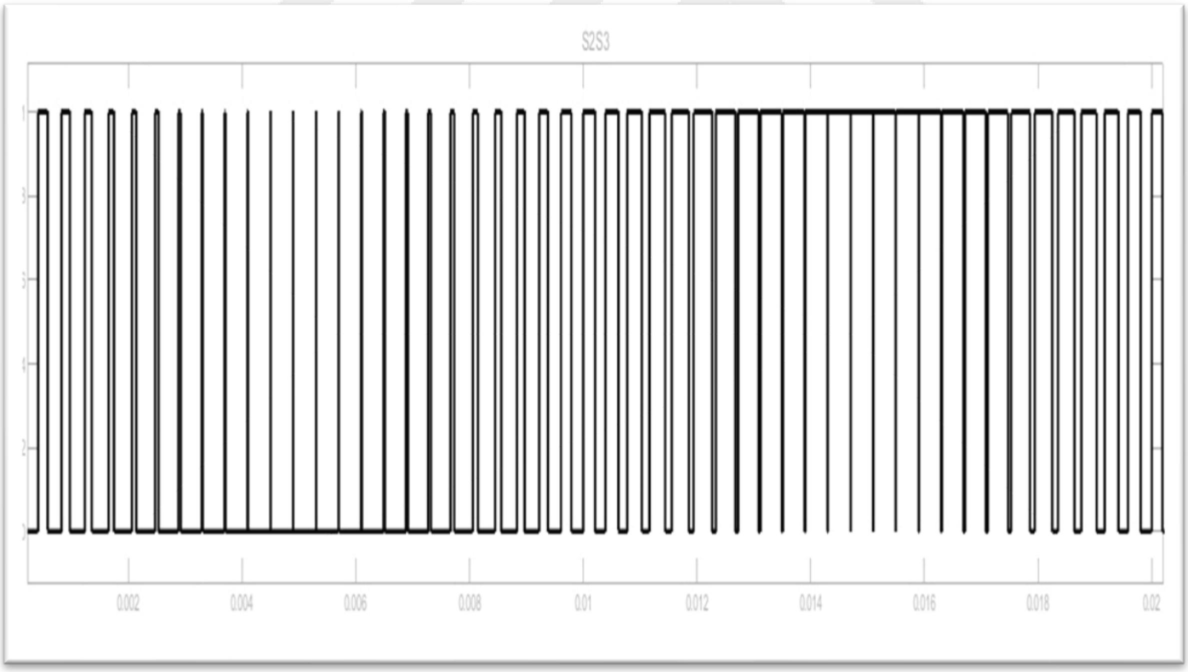

Figure 3.14: Bipolar PWM gating pulses for S2 and S3

4. CONTROL ALGORITHM OF PROPOSED METHOD

The available resources on the mathematical analysis and modelling of the Zeta converter are notably limited. The existing literature often treats mathematical analysis and modelling as separate subjects, resulting in the absence of a comprehensive source that addresses both aspects together. Moreover, the resources that do discuss modelling often lack detailed explanations and contain inaccuracies (Babu et al., 2015). In this study, it is aimed to fill this gap by presenting both the theoretical framework and practical application of the Zeta converter. For the first time in the literature, both the theoretical and practical aspects are examined in a unified manner. The functionality of both applications has been verified and validated. To ensure accurate results, the Ziegler-Nichols method and the Routh-Hurwitz criterion were employed. The MATLAB codes utilized for these methods are provided in the appendix section of this thesis.

4.1. Ziegler-Nichols Method

The Ziegler-Nichols Method is widely used for tuning PID (Proportional-Integral-Derivative) controllers in automatic control systems. Developed by John G. Ziegler and Nathaniel B. Nichols in 1942, the method aims to determine the PID parameters that will provide optimal performance for control systems (Ziegler, J. G. and N. B. Nichols., 1942).

Ziegler and Nichols introduced straightforward mathematical procedures, commonly referred to as the first and second methods, for tuning PID controllers. These procedures have since become standard practice in control systems engineering. Detailed discussions on various PID controller tuning methods are provided below. (Ziegler, J. G. and N. B. Nichols., 1942).

4.1.1 Step Response (Open Loop) Method

The step response method utilizes the system's step response to determine the PID parameters. In this approach, the system is subjected to a unit step input, and the resulting response curve (reaction curve) is recorded. This method, based on an open-loop step response test of the process, necessitates the stability of the process. The unit step response is characterized by two critical parameters: the delay time (L) and the time constant (T). These parameters are calculated by drawing a tangent line at the inflection point of the step response curve, where the slope reaches its maximum value. The intersections of this tangent line with the coordinate axes yield the process parameters L and T. These values are then employed to derive the PID controller parameters, as illustrated in Figure 4.1. (K. J. Åström., et al., 2004).

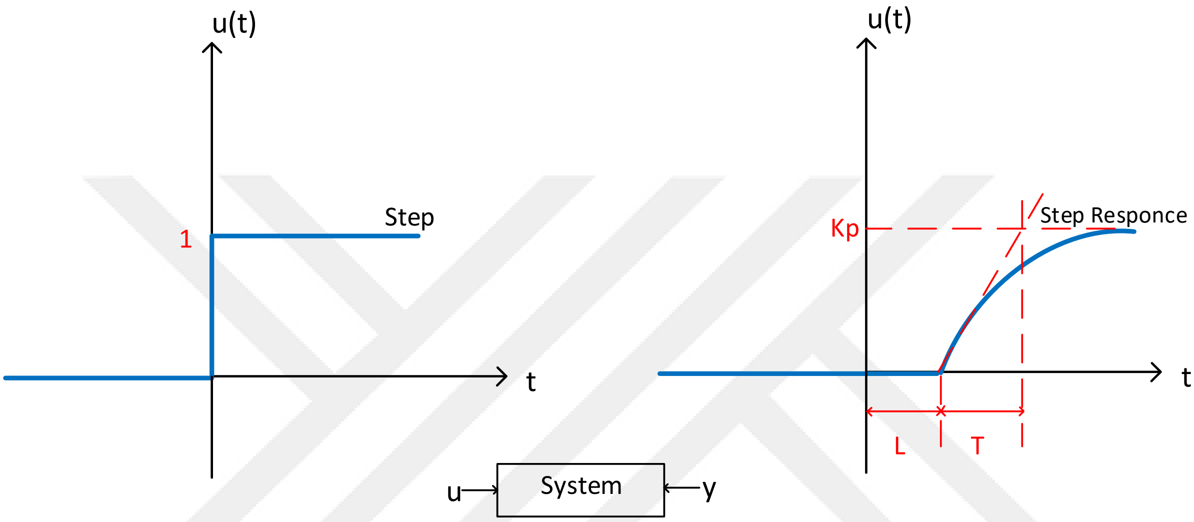

Figure 4.1: Nichols step response methods response curve

Table 4.1 displays the PID, PI, and controller parameters that were obtained by applying the Ziegler-Nichols step response approach.

Table 4.1: Ziegler-Nichols recipe – step response method

Control Type	K_p	T_i	T_d
P	T/L		
PI	0.9T/L	L/0.3	
PID	1.2T/L	2L	0.5L

4.1.2 Closed Loop (Critical Oscillation) Method

The Critical Oscillation Method, also known as the Closed-loop Method, is a technique used for tuning PID controllers in control systems engineering. This method involves operating the control system in a closed-loop configuration to determine optimal PID parameters.

The procedure entails the following steps:

- Begin by setting the proportional control (K_p).
- Incrementally increase the proportional gain (K_p) until the system exhibits instability, characterized by sustained oscillations, indicating the critical gain value (K_{cr}).
- Measure the oscillation period to determine the critical time constant (P_{cr}).
- With K_{cr} and P_{cr} values determined, calculate the PID parameters according to the design specifications outlined in Table 4.2. (K. J. Åström., et al., 2004).

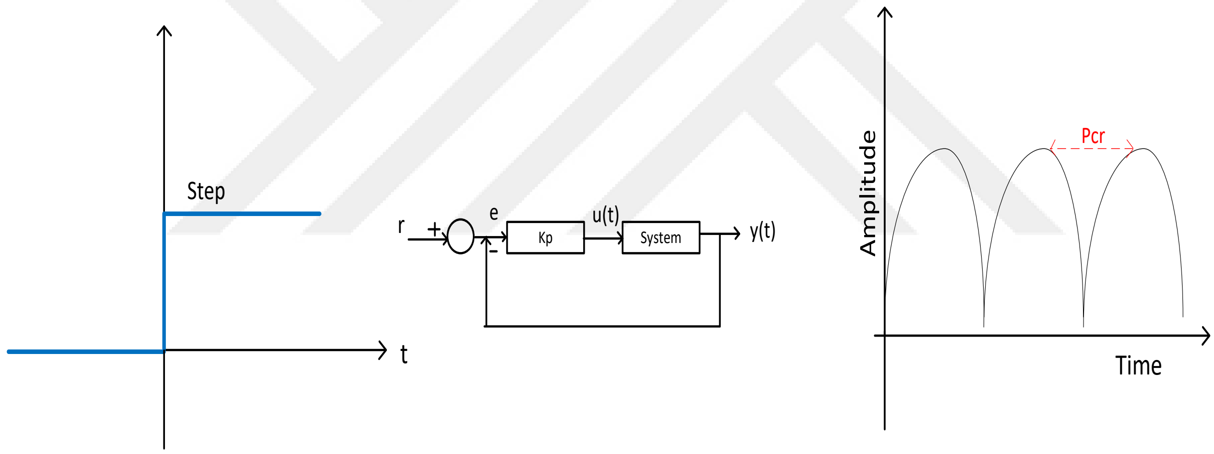

Figure 4.2: Response curve for Ziegler-Nichols closed loop method

Table 4.2: Ziegler-Nichols recipe – closed loop method

Control Type	K_p	T_i	T_d
P	0.5* K_{cr}		
PI	0.45* K_{cr}	P_{cr}/1.2	
PID	0.6* K_{cr}	0.5* P_{cr}	0.125* P_{cr}

4.2. Routh-Hurwitz Method

The Routh-Hurwitz method is a classical approach in control theory for determining the stability of linear systems. This method evaluates the system's stability by examining the coefficients of its characteristic polynomial. (Ogata, K., 2010).

4.2.1. Fundamental Principles:

Characteristic Polynomial:

- This method utilizes the system's characteristic polynomial expressed as
- The stability of the system is inferred from the location of the roots of this polynomial.

Routh Table:

- The Routh-Hurwitz criterion necessitates creating a Routh array using the coefficients of the characteristic polynomial.
- The first two rows of the array are populated directly from the polynomial's coefficients.
- Subsequent rows are calculated using specific rules involving the coefficients from the previous rows.

Stability Criterion:

- The number of sign changes in the first column of the Routh table indicates the number of roots with positive real parts.
- If no sign changes occur in the first column of the Routh array, the system is stable. Otherwise, the system is unstable.

The transfer function was calculated using the MATLAB code provided in Appendix A of the thesis.

Transfer function is:

$$\frac{Vout(S)}{Vin(S)} = \frac{7.051\text{e}07s^2 - 1.742e{-}06s + 3.688e13}{s^4 + 1.175e04s^3 + 1.01e08s^2 + 1.217e10s + 1.543e13} \quad (4.1)$$

The converter's transfer function can be formulated as follows:

$$G(S) = \frac{7.051\text{e}07s^2 - 1.742e{-}06s + 3.688e13}{s^4 + 1.175e04s^3 + 1.01e08s^2 + 1.217e10s + 1.543e13} \quad (4.2)$$

To derive the quadratic equation using the transfer function, proceed as follows:

H(S) = Feedback gain (4.3)

H(S) = 1 (4.4)

1+G(S)H(S)=0 (4.5)

Then

$$\mathbf{1} + \frac{7.051\text{e}07s^2 - 1.742e{-}06s + 3.688e13}{s^4 + 1.175e04s^3 + 1.01e08s^2 + 1.217e10s + 1.543e13} = \mathbf{0} \quad (4.6)$$

Upon solving the equation, we derive the characteristic equation.

By substitute s=jω and equating the real terms, we find the value of ω

(4.7)

$P_{cr} = (9.35*10^{-3})$ (4.8)

The closed-loop transfer function's denominator polynomial, in the presence of K_{cr}, was analysed using the Routh-Hurwitz method to determine the value of K_{cr} that stabilizes the system. Based on the coefficients of the denominator polynomial associated with K_{cr}, the stability of the system was assessed. Detailed code for this calculation is provided in Appendix B of the thesis.

$K_{cr} = 0.0153$ (4.9)

The proportional gain constant will be as follows:

$K_P = 0.6*K_{cr}$ (4.10)

$K_p = 0.0092$ (4.11)

In a similar manner for;

$K_i = K_p / T_i$ (4.12)

$K_i = 16.6$ (4.13)

In a similar manner for ;

$K_d = K_p*T_d$ (4.14)

$K_d = 9.31*10^{-5}$ (4.15)

5. SIMULATION CASE STUDIES

5.1. MATLAB/Simulink Model of Zeta Converter

Simulation results using MATLAB-Simulink software are shown to validate the performance of the Zeta Converter topology specified. The proposed Zeta Converter topology has been tested with various case studies. The overall MATLAB/Simulink model of the proposed Zeta Converter topology is shown in Figure 4.1. The design parameters and control parameters used in the simulation model are provided in Table 4.1 - Table 4.4. The control algorithms for the Zeta Converter circuit specified in Section 3 were developed using the MATLAB editor to reduce simulation complexity. This simulation study aims to achieve the following features by examining various case studies:

- Examining the system's response across different voltage levels
- Analyzing both the steady-state and dynamic behaviour under varying load conditions

Table 5.1. MATLAB/Simulink Simulation Parameters

MATLAB/Simulink Parameters
Solver Maximum Step Size: 5e-07 s
Duration of Simulation Time: 8 s

Table 5.2. Control System Parameters

DC-Link PI Control Parameters
Kp: 0.0092
Ki: 16.6

Table 5.3. System Parameters of Zeta Converter

Parameter	**Value**
f_s	50kHz
C	480µF
C_2	8.51µF
L_1	1.175µH
L_2	1.175µH
Turn Ratio (V_1/V_2)	12/220

Table 5.4. System Parameters of Proposed System

Parameter	**Value**
f_s	50kHz
C	480µF
C_2	8.51µF
L_1	1.175µH
L_2	1.175µH
R (Zeta Converter)	1000 Ω
R	250 Ω

In accordance with the parameters given in Table 5.4, the circuit targeted in this study was designed in MATLAB. In this circuit, the input voltage was selected as 5v, and the output voltage was obtained as 12v in the zeta converter. The output voltage remained at the same desired value against the variable input voltage. Then, the 12v DC voltage was converted to 12v AC voltage with the single-phase h-bridge inverter used. Then, the 12v AC voltage was increased to 220v AC voltage with the transformer used. In the intended circuit, 24A ZK current is taken as basis.

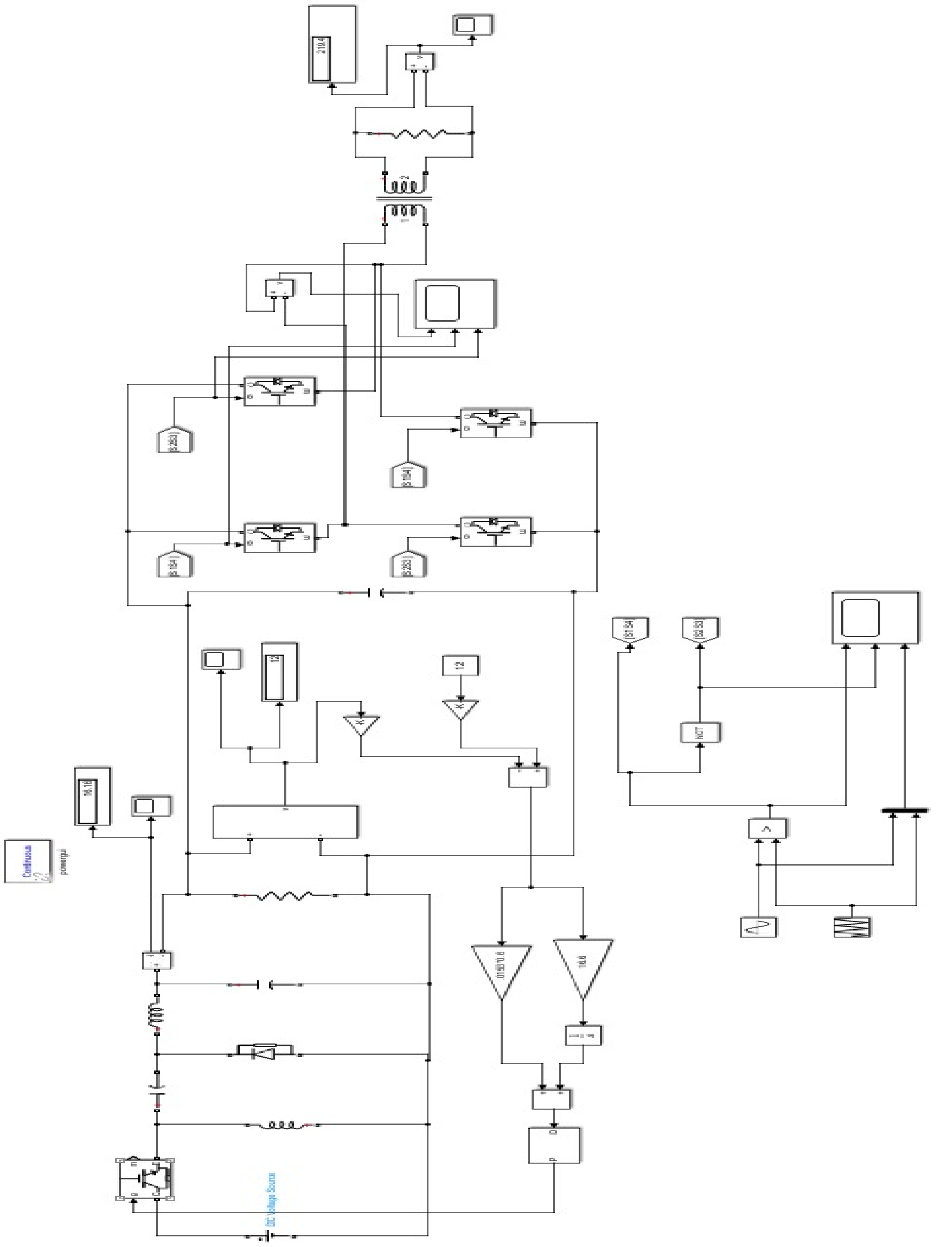

Figure 5.1. The simulation model of the proposed system

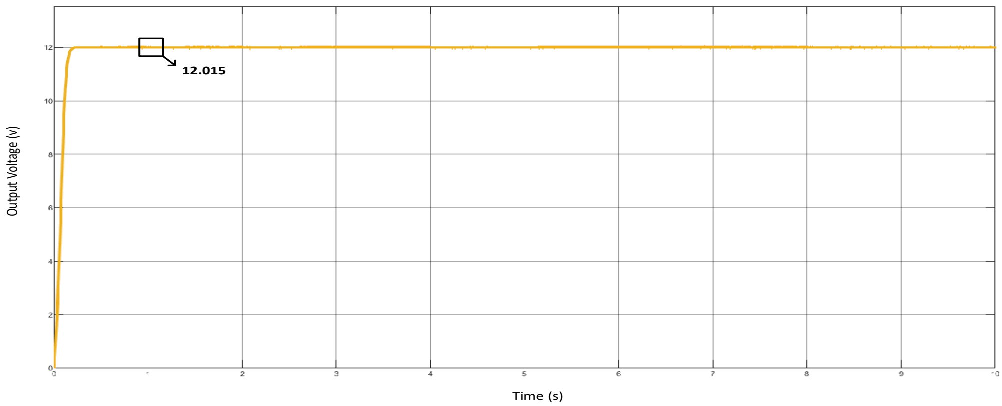

Figure 5.2. Zeta converter output voltage of proposed system

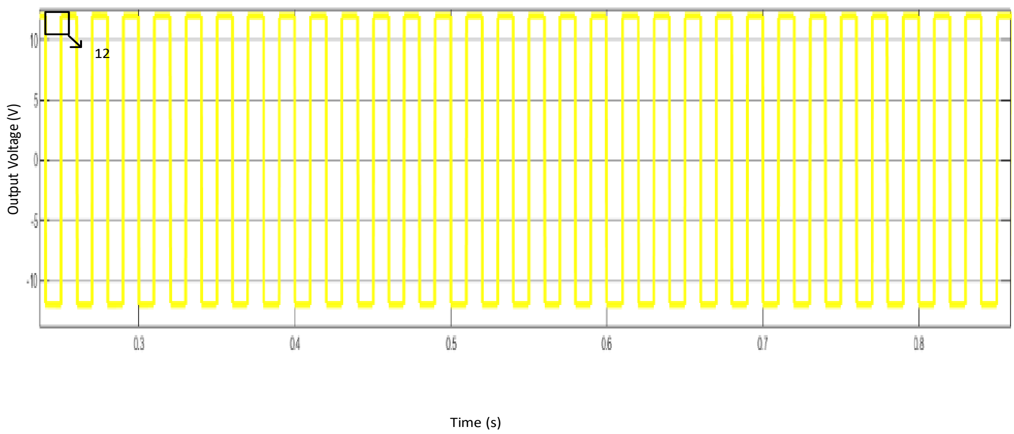

Figure 5.3. Inverter output voltage of the proposed system

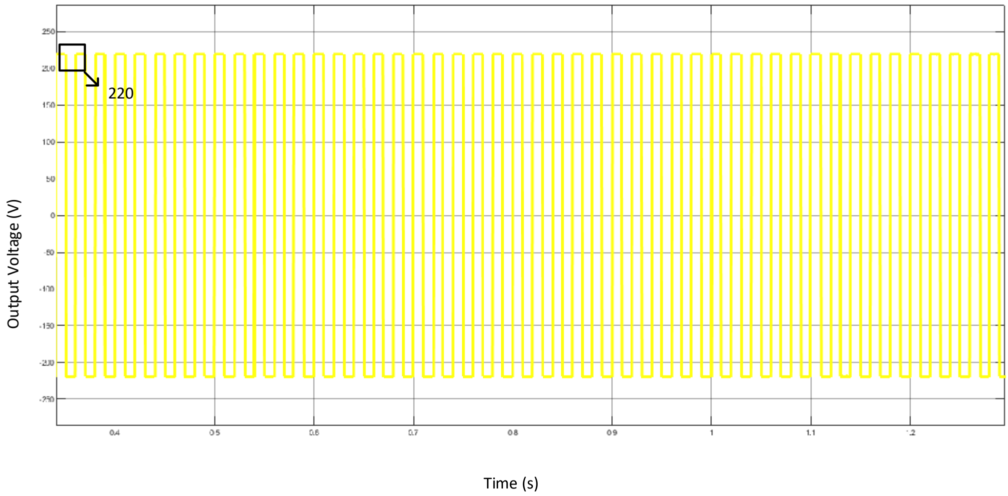

Figure 5.4. Transformer output voltage of the proposed system

This section details the simulation model of the proposed system along with the results obtained from various case studies. To assess the effectiveness and feasibility of the proposed converter, three case studies were conducted, which are summarized in Table 5.5.

Table 5.5. Summary of Case Studies

Case Studies	Parameter	Value
Case Study #1	V_{IN}	5V
	V_{OUT}	12V
	Resistance	10Ω
Case Study #2	V_{IN}	12V
	V_{OUT}	12V
	Resistance	10Ω
Case Study #3	V_{IN}	18V
	V_{OUT}	12V
	Resistance	10Ω
Case Study #4	V_{IN}	12V
	V_{OUT}	12V
	Resistance	20Ω
Case Study #5	V_{IN}	12V
	V_{OUT}	12V
	Resistance	5Ω
Case Study #6	V_{IN}	12V
	V_{OUT}	12V
	Resistance	2Ω

5.2. Case Study 1

The first case study focuses on maintaining the output voltage at 12v with an input voltage of 5v, followed by emphasizing the output using a sinusoidal pulse width modulation inverter.

However, the output graphs of the Zeta Converter are provided in the following figures. The performance of the proposed system was examined by varying the voltage range. The values used are based on those provided in Table 5.4 for Case Study 1.

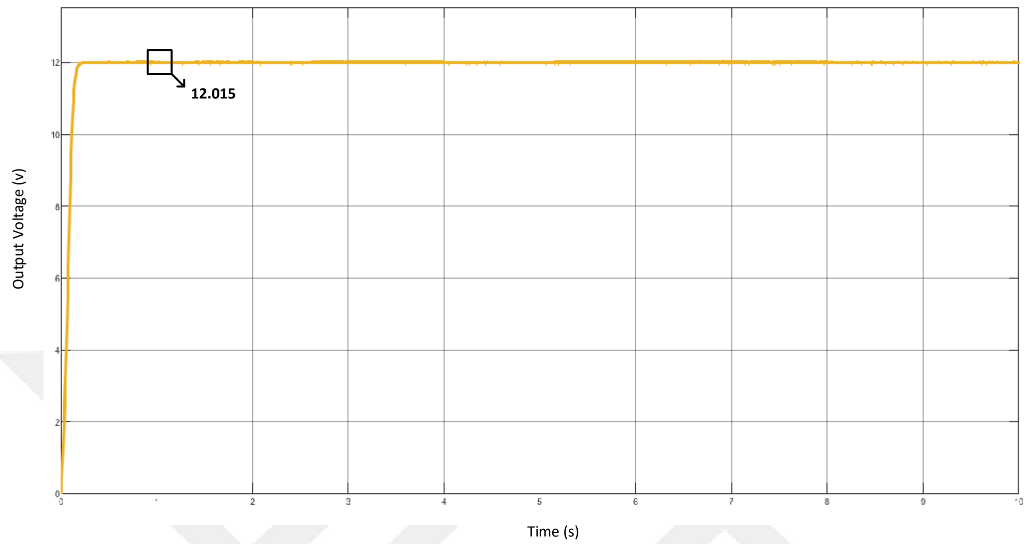

Figure 5.5. Zeta converter output voltage of case study1

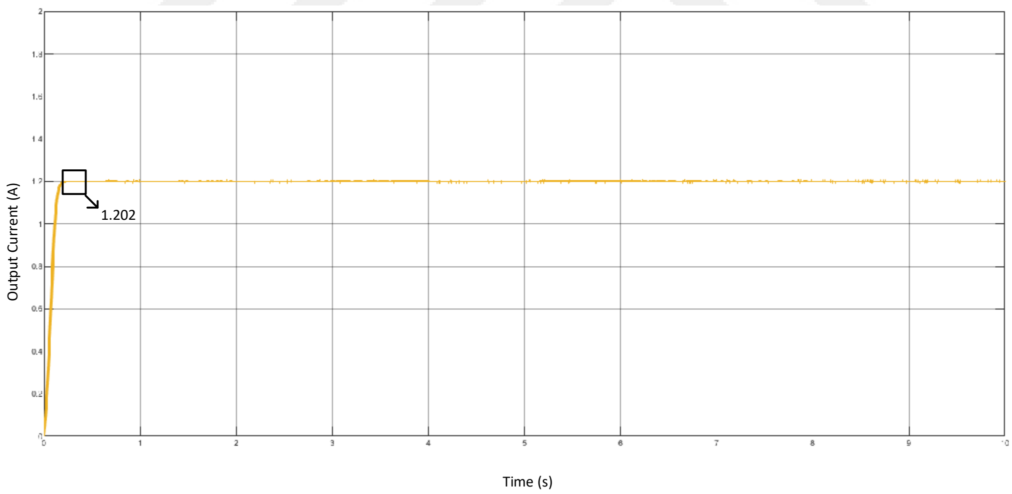

Figure 5.6. Zeta converter output current of case study1

5.3 Case Study 2

The second case study focuses on maintaining the output voltage at 12v with an input voltage of 12v, followed by emphasizing the output using a sinusoidal pulse width modulation inverter. However, the output graphs of the Zeta Converter are provided in the following figures. The performance of the proposed system was examined while keeping the voltage range constant. The values used are based on those provided in Table 5.4 for Case Study 2.

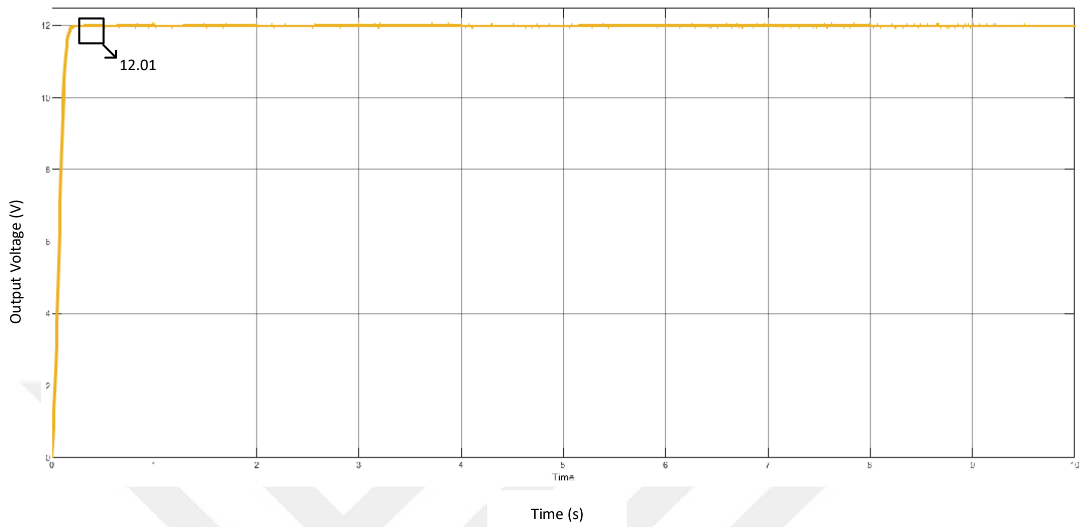

Figure 5.7. Zeta converter output voltage of case study2

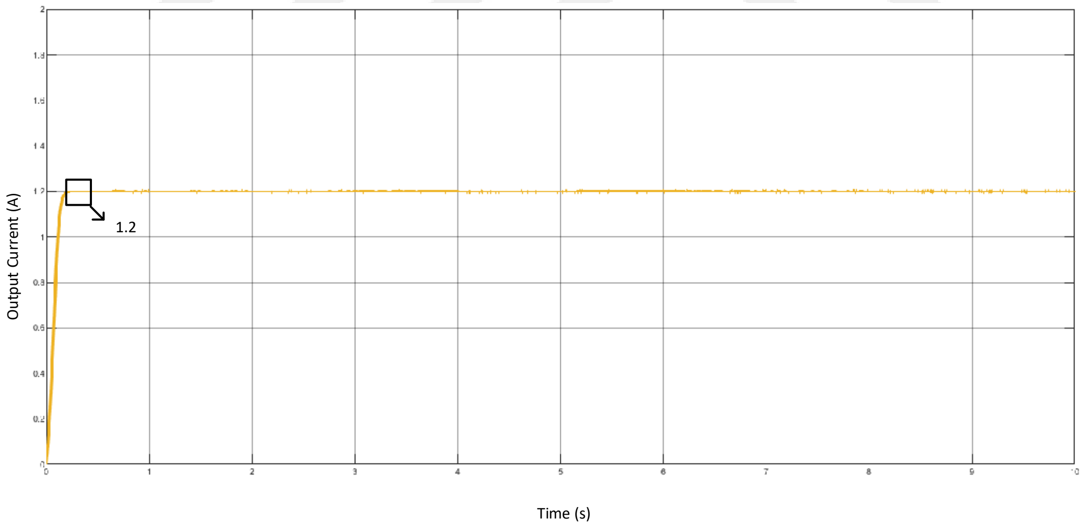

Figure 5.8. Zeta converter output current of case study2

5.4 Case Study 3

The second case study focuses on maintaining the output voltage at 18v with an input voltage of 12v, followed by emphasizing the output using a sinusoidal pulse width modulation inverter. However, the output graphs of the Zeta Converter are provided in the following figures. The performance of the proposed system was examined while keeping the voltage range constant. The values used are based on those provided in Table 5.4 for Case Study 3.

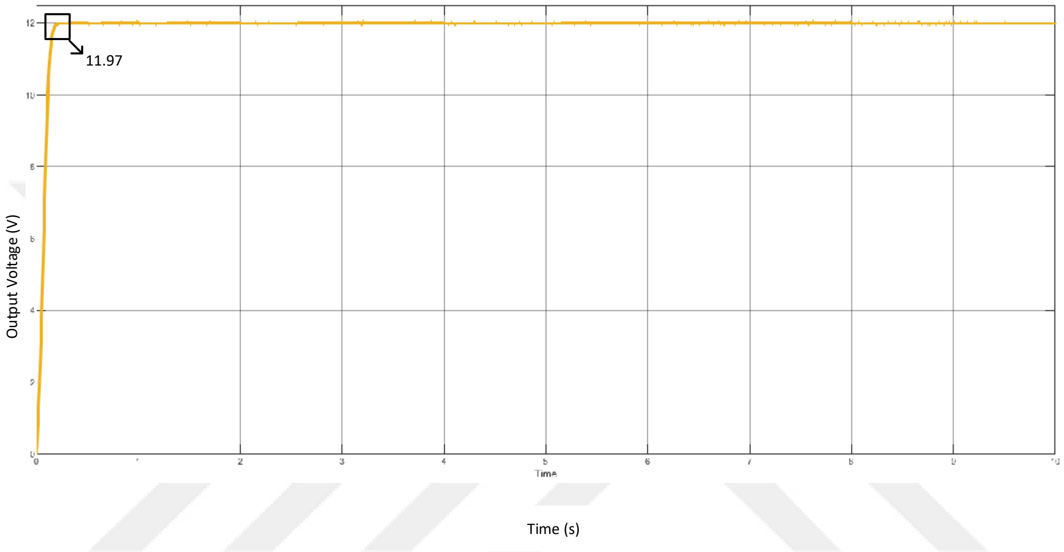

Figure 5.9. Zeta converter output voltage of case study3

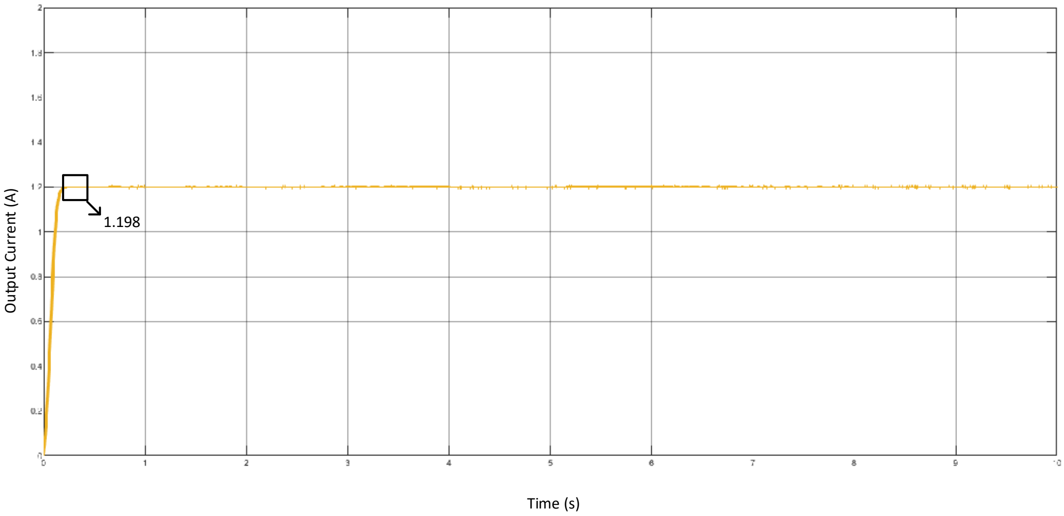

Figure 5.10. Zeta converter output current of case study3

By incorporating the three case studies, along with an analysis of the dynamic response for a 15v input voltage, this study aims to evaluate the stability of the output voltage under varying input conditions. This approach will enable a detailed observation of the control system's behaviour.

5.5 Case Study 4

The third case study focuses on maintaining the output voltage at 12v with an input voltage of 12v. Unlike other case studies, the value of the resistor is changed from 10 ohms to 20 ohms. The performance of the proposed system was examined by keeping the voltage range constant. Accentuation of the output was followed using an inverter with sinusoidal pulse width modulation. However, the output graphs of Zeta Converter are given in the figures below. The values used are based on those given in Table 5.4 for Case Study 4.

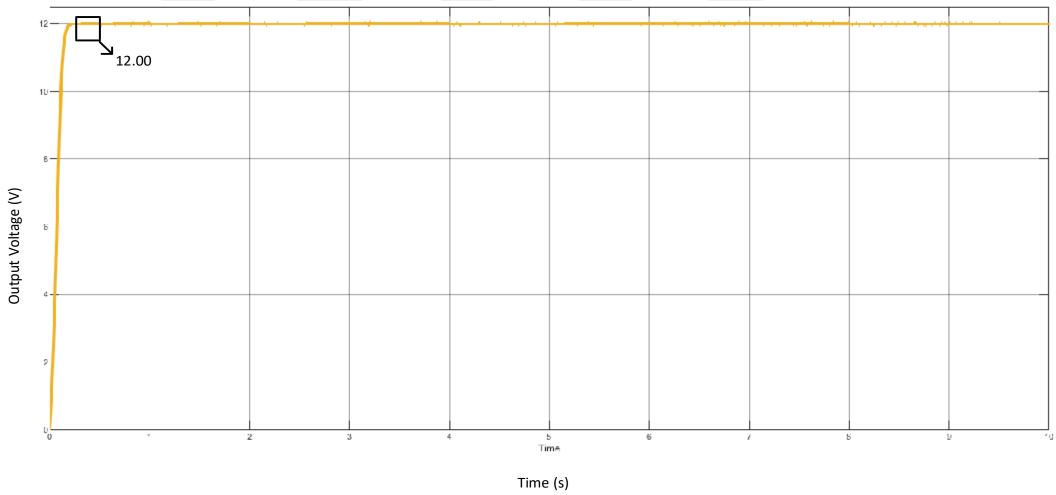

Figure 5.11. Zeta converter output voltage of case study4

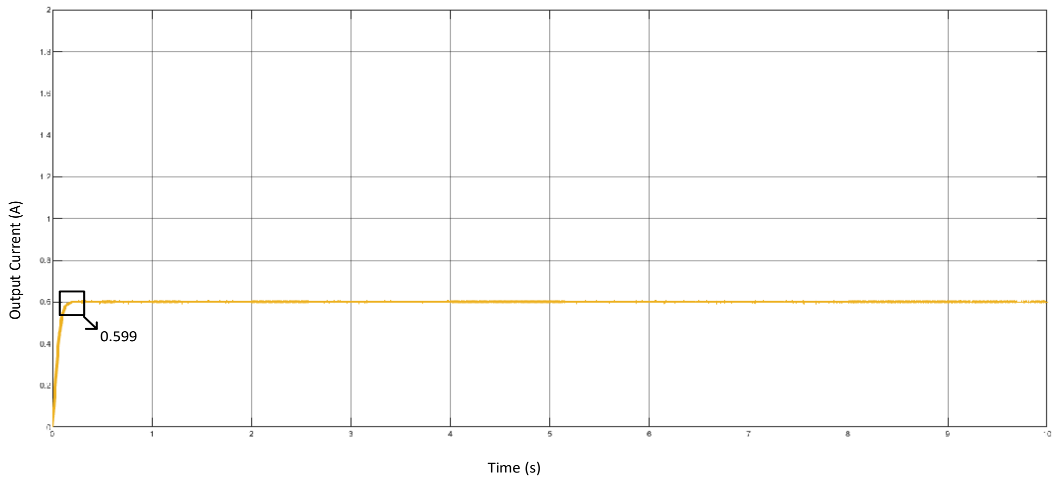

Figure 5.12. Zeta converter output current of case study4

5.6 Case Study 5

The fourth case study focuses on keeping the output voltage at 12v with an input voltage of 12v. Unlike other case studies, the value of the resistor was changed from 10 ohms to 5 ohms. The performance of the proposed system was examined by keeping the voltage range constant. The acceleration of the output was monitored using an inverter with sinusoidal pulse width modulation. However, the output graphics of Zeta Converter are given in the figures below. The values used are based on those given in Table 5.4 for Case Study 5.

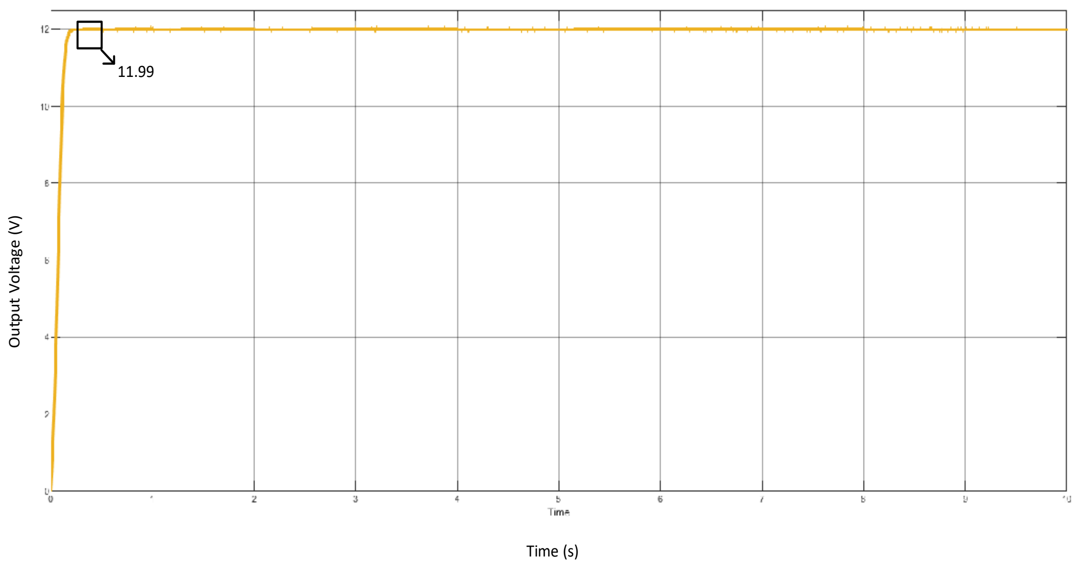

Figure 5.13. Zeta converter output voltage of case study5

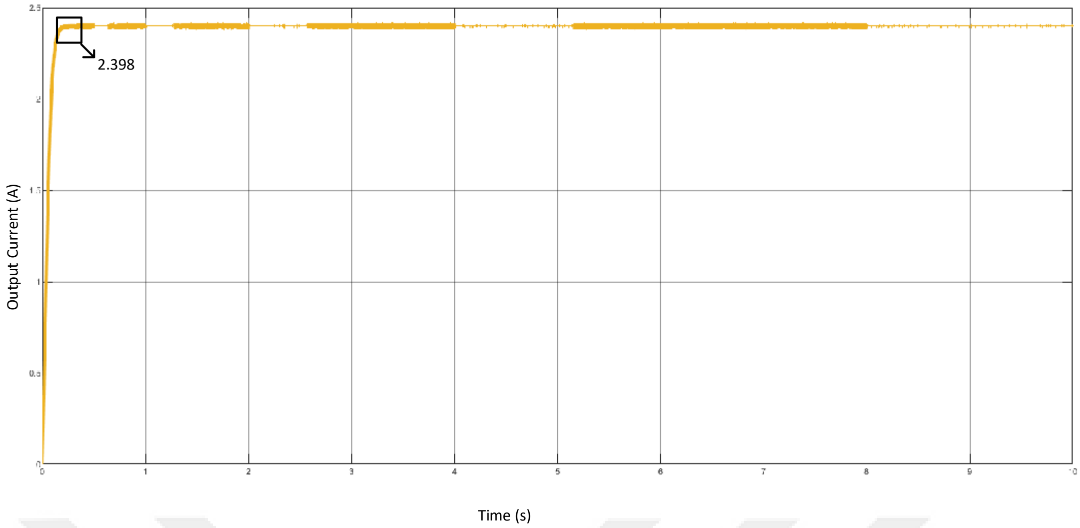

Figure 5.14. Zeta converter output current of case study5

5.7 Case Study 6

The fifth case study focuses on keeping the output voltage at 12v with an input voltage of 12v. Unlike other case studies, the value of the resistor was changed from 10 ohms to 2 ohms. The performance of the proposed system was examined by keeping the voltage range constant. The acceleration of the output was monitored using an inverter with sinusoidal pulse width modulation. However, the output graphics of Zeta Converter are given in the figures below. The values used are based on those given in Table 5.4 for Case Study 6.

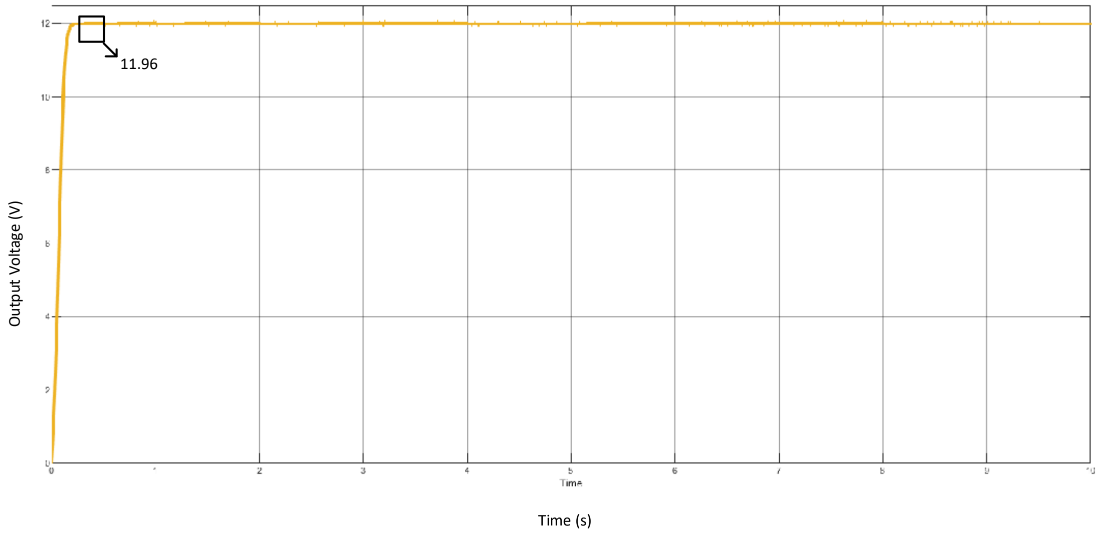

Figure 5.15. Zeta converter output voltage of case study6

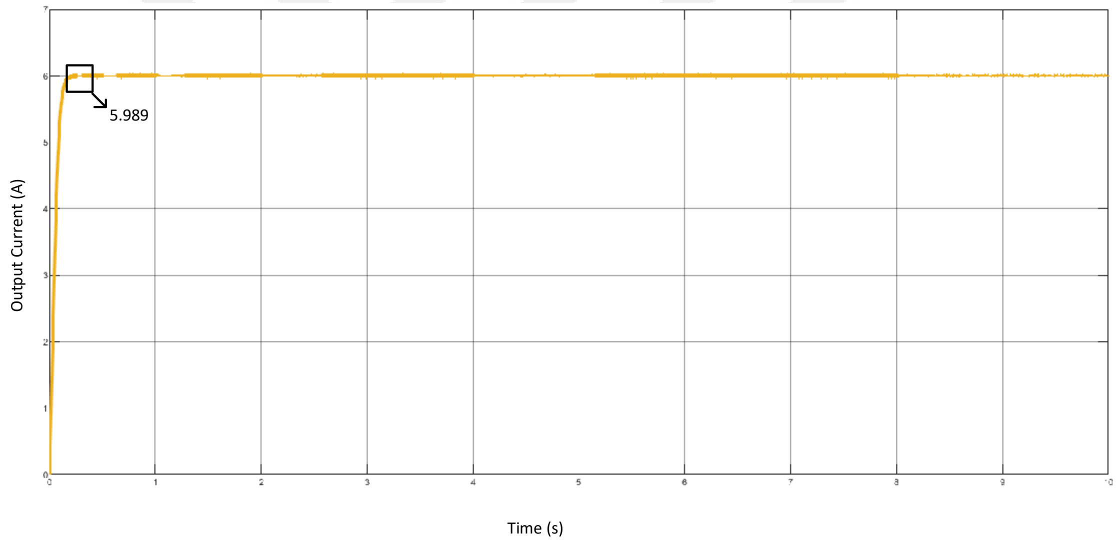

Figure 5.16. Zeta converter output current of case study6

5.8 Summary

Six case studies were carried out to assess the effectiveness and feasibility of the proposed simulation. These case studies involved varying the input voltage and were designed to validate all operating modes of the proposed system.

Considering the reviewed case studies, we can clearly see that without changing the resistor value, there is no major change in the output current due to the variable input voltage. This shows that whether we choose our input voltage between 5v and 18v, the output current does not change much. Of course, in this case, our circuit continues to keep the output voltage at the desired value, that is, 12v. On the other hand, when we examine case study 4-5-6, we can see that there are obvious differences in our output current depending on the constant input voltage versus variable resistor values. By changing our resistance in the range of 2-20 ohms, we see that the output current increases as the resistance value decreases. Of course, our output voltage still remains at the desired value.

6. CONCLUSIONS

The objective of this thesis was to use SPWM technique in conjunction with a fluctuating DC input voltage to produce a steady DC output voltage that could be used for AC consumption. Firstly, the modelling of the zeta converter was conducted, and simulations were performed to examine its performance under various input voltages. These simulations demonstrated that the zeta converter could operate stably and efficiently.

Additionally, the control methods for the zeta converter were thoroughly examined, and optimization was achieved using various algorithms. Within this scope, the effectiveness of the control algorithms was tested, and necessary adjustments were made to achieve the desired stable output voltage corresponding to the desired input voltage. The obtained results were consistent with theoretical analyses, revealing how the zeta converter behaves under different conditions.

The studies conducted within this thesis have provided a comprehensive examination of the zeta converter by integrating modelling, control, and simulation phases that were not previously presented together in the literature. Furthermore, the control algorithms used in this study and the results obtained are presented for the first time both theoretically and practically in the literature. Therefore, this study makes a significant contribution to the field of electrical and electronics engineering.

In conclusion, this thesis has demonstrated the effectiveness of zeta converters in achieving a stable output voltage from variable input voltages and has shown that AC usage can be obtained using the PWM method. These findings offer new perspectives for the development and optimization of energy conversion systems.

7. APPENDIX FUNCTION

7.1. Appendix A

```
D=0.705;

L1=1.175e-3;

L2=1.175e-3;

C1=4.8e-4;

C2=8.51e-6;

R=10;

As= [0 0 (D-1)/L1 0;0 0 D/L2 -1/L2;(1 -D)/C1 -D/C1 0 0;0 1/C2 0 -1/(R*C2)];

Bs= [D/L1; D/L2; 0; 0];

Cs= [0 0 0 1];

Ds= [0];

Vs= 5;

[Num, den]= ss2tf(As,Bs,Cs,Ds)

sys= tf(Num,den)

step (sys*Vs)

grid
```

7.1. Appendix B

```
%%%Routh Hurwitz Automatically

clear

clc

close all

syms K % - hey if you have the symbolic toolbox try this

coeff = [1,1.175e04,1.01e08,1.217e10, 1.543e13+K]

%%%%Create the First Row of the Routh Table

routh_table = [];

first_row = [];

for idx = 1:2:length(coeff)

    first_row = [first_row,coeff(idx)];

end

while length(first_row) <= 2

    first_row = [first_row,0];

end

disp('First Row')

routh_table = [routh_table;first_row]

%%%%Create the second row of the Routh Table

second_row = [];

for idx = 2:2:length(coeff)
```

```
    second_row = [second_row,coeff(idx)];
end
while length(second_row) < length(first_row)
    second_row = [second_row,0];
end
disp('Second Row')
routh_table = [routh_table;second_row]
routh_table_width = length(first_row);
%%%Now create the next rows
required_rows_to_compute = length(coeff)-2;
%%%Check and see if this is first order or smaller
if required_rows_to_compute < 0
    disp('Trivial Solution')
    return
end
for loop_row = 1:required_rows_to_compute
    row = [];
    %disp(['Computing Row ',num2str(loop_row+2)])
    disp('Divide All Determinants by this var = ')
    divisor = routh_table(loop_row+1,1)
    %%THe left part of the determinant for a given row is constant
```

```
    %Thanks Sumit Godara for pointing that out
    %disp('Left Half Determinat')
    left_half_det = routh_table(loop_row:loop_row+1,1);
    for col = 1:routh_table_width
        %disp(['Computing Column ',num2str(col)])
        if col == routh_table_width
            right_half_det = [0;0];
        else
            right_half_det = routh_table(loop_row:loop_row+1,col+1);
        end
        disp('Determinant to be computed')
        both_det = [left_half_det,right_half_det]
        value = -det(both_det)/divisor;
        row = [row,value];
    end
    disp('Next Row of Routh Table')
    routh_table = [routh_table;row]
end
%%%Check for stability
%%%Grab the first column
routh_table
```

```
first_column = routh_table(:,1)

s = sign(first_column(1));

unstable = 0;

for idx = 2:length(first_column)

    value = first_column(idx);

    if s ~= sign(value)

        disp('Unstable ')

        unstable = 1;

        break

    end

end

if ~unstable

    disp('System is Stable')

end
```

REFERENCES

Aboadla E, H. E., Khan, S., Habaebi, H. M., Gunawan, T., Hamidah, A. B., Yaacob, B. M. (2016). Effect of modulation index of pulse width modulation inverter on Total Harmonic Distortion for Sinusoidal. 2016 International Conference on Intelligent Systems Engineering (ICISE), Islamabad, Pakistan, 2016, pp. 192-196, doi: 10.1109/INTELSE.2016.7475119.

Aiello, M. F., Hammond, P. W., Rastogi, M. (2001). Modular multi-level adjustable supply with parallel connected active inputs, US Patent 3 867 643, 1–13.

Alamri, B., Alshahrani, S., Darwish, M. (2015). Losses investigation in SPWM-controlled cascaded H-bridge multilevel inverters. 2015 50th International Universities Power Engineering Conference (UPEC), Stoke on Trent, UK, 2015, pp. 1-5, doi: 10.1109/UPEC.2015.7339805.

Albu, R. D., Gordan C. E. (2021). Counting Atypical Metal Pieces System. An Eddy Currents approach. 16th International Conference on Engineering of Modern Electric Systems (EMES), 10-11 June 2021, pp. 1-4, DOI: 10.1109/EMES52337.2021.9484155.

Albu, D. R., Gordan, C. E. (2023). Single-Phase SPWM Inverter Ordered with Microcontroller. 2023 17th International Conference on Engineering of Modern Electric Systems (EMES), Oradea, Romania, 2023, pp. 1-5, doi: 10.1109/EMES58375.2023.10171665.

Alkhazragi. S. M., K.AL-Shamaa, N. (2017). Int. Journal of Engineering Research and Application, ISSN: 2248-9622, Vol. 7, Issue 6, (Part -2) June 2017, pp.14-20

Ankit., Sahoo., K, S., Sukchai, S., Yanine, F. F. (2018). Review and comparative study of single-stage inverters for a PV system. Renewable And Sustainable Energy Reviews, 91 (2018): 962–986 (2018).

Antar, K. R. (2018). Multilevel inverter with unequal and selected DC voltage sources using modified absolute sinusoidal PWM technique. 2018 1st International Scientific Conference of Engineering Sciences - 3rd Scientific Conference of Engineering Science (ISCES), Diyala, Iraq, 2018, pp. 62-67, doi: 10.1109/ISCES.2018.8340529.

Arab, M. (2014). Micro-controlled Pulse Width Modulator Inverter for Renewable Energy Generators. Energy Procedia 50 (2014): 832-840.

Aström, K. J., Hägglund, T. (2004). Revisiting the Ziegler-Nichols step response method for PID control. Journal of Process Control, Vol. 14, pp. 635-650, 2004.

Babu, P. R., Prasath, S. R., Kiruthika R. (2015). Simulation and performance analysis of CCM Zeta converter with PID controller. 2015 International Conference on Circuits, Power and Computing Technologies [ICCPCT-2015], Nagercoil, India, 1-7, doi: 10.1109/ICCPCT.2015.7159506.

Baker, R. H., Bannister, L. H. (1975). Electric power converter.

Baker, R. H., Bedford, Mass. (1981). Bridge converter circuit, United States Patent, 54–55.

Barge, Arvind, S., Jagtap, S. R. (2013). Harmonic Analysis of Sinusoidal Pulse Width Modulation. International Journal of Advanced Electrical and Electronics Engineering 2.5 (2013): 13- 16.

Bowtell, L., Ahfock, T. (2007). Compari - son Between Unipolar and Bipolar Sigle Phase Grid connected Inverters for PV Applications. September 20, 2007.

Durgadevi, K., Karthik, R. (2018). Performance Analysis of Zeta Converter Using Classical PID and Fractional Order PID Controller. 2018 International Conference on Power, Energy, Control and Transmission Systems (ICPECTS), Chennai, India, 2018, pp. 312-317, doi: 10.1109/ICPECTS.2018.8521573.

Erickson, R. W., Maksimovic, D. (2004). Fundamentals of power electronics, Second Edition, Kluwer Academic Publishers.

Garg, M. M., Hote, Y. V., Pathak, M. K. (2015). PI controller design of a DC-DC Zeta converter for specific phase margin and cross-over frequency. 2015 10th Asian Control Conference (ASCC), Kota Kinabalu, Malaysia, 2015, pp. 1-6, doi: 10.1109/ASCC.2015.7244716.

Jana, J., Saha, H., Bhattacharya, K. (2017). A review of inverter topologies for single-phase grid-connected photovoltaic systems. Renewable And Sustainable Energy Reviews, 72 (October 2016): 1256–1270 (2017).

Jozwik, J. J., Kazimierczuk, M. K. (1989). Dual SEPIC PWM switching-mode DC/DC power converter. IEEE Transactions on Industrial Electronics, 36(1): 64-70.

Jung, E., Seung-kiSul. (2009). Implementation of Grid-connected Single Phase Inverter Based on FPGA. 24th Annaul IEEE Conference on Applied Power Electronics and Expostion, 2009, pp. 889-893

Ioinovici, A. (2013). Power electronics and energy conversion systems, fundamentals and hard-switching converters, I, John Wiley & Sons.

Ismail, B., Saad, M. R., Isa, M., Taib, S. (2006). Development of A Single Phase Spwm Microcontroller-Based Inverter. First International Power and Energy Coference Pecon 2006 November 28-29, 2006, Putrajaya, and Malasia .PN.437-440.

Khaleghi, H., Varjani, A. Y., Mohamadian, M. (2014). A new bidirectional Zeta DC/DC converter. The International Power Electronics, Drive Systems and Technologies Conference, 5-6 February 2014, Tehran, 131-136.

Lai, J-S., Peng, F. Z. (1996). Multilevel converters-a new breed of power converters, IEEE Transactions on Industry Applications, 32, 3, 509–517.

Liao, Z., Cao, C., Qiu, D. (2019). Analysis on topology derivation of single-phase transformerless photovoltaic grid-connect inverters. Optik, 182 (December 2018): 50–57 (2019).

Lin, J. L., Yang, S. P., Lin, P. W. (2005). Small-signal analysis and controller design for an isolated zeta converter with high power factor correction. Electric Power Systems Research, 76(1): 67-76.

Ma, J., Wang, X., Blaabjerg, F., Song, W., Wang, S., Liu, T. (2020). Real-Time Calculation Method for Single-Phase Cascaded H-Bridge Inverters Based on Phase-Shifted Carrier Pulsewidth Modulation. in IEEE Transactions on Power Electronics, vol. 35, no. 1, pp. 977-987, Jan. 2020, doi: 10.1109/TPEL.2019.2911422.

Martins, D. C., De Abreu, G. N. (1993). Application of the ZETA converter in switch-mode power supplies. Applied Power Electronics Conference and Exposition, 7-11 March 1993, San Diego, 214-220.

Mazumder, K., Mahbub, M., Rahman, M., Amin, G. (2017). Design and Analysis of DC-DC PWM Converter and DC-AC Converter.

Mohan, N., Undeland, T. M., Robbins, W. P. (1995). Power electronics: converters, applications, and design, Second Edition, John Wiley & Sons.

Molina, M. G. (2016). Modelling and Control of Grid-connected Solar Photovoltaic Systems. Renewable Energy - Utilisation and System Integration, InTech, 53–83 (2016).

Nabae, A., Takahashi, I., Akagi, H. (1981). A New Neutral-Point-Clamped PWM Inverter, IEEE Transactions on Industry Applications, IA-17, 5, 518–523.

Nagarajan, R., Yuvaraj, R., Kumar, K., Babu, D, R. (2016). Implementatıon Of SPWM Technıque for Inverter. International Journal of Advanced Research in Biology, Engineering, Science and Technology, (IJARBEST), Vol. 2, Issue 9, September 2016

Namboodiri., Anuja., Wani, S. H. (2015). Unipolar and Bipolar PWM Inverter. International Journal for Innovative Research in Science and Technology 1.7 (2015): 237-243.

Niculescu, E., Iancu, E. P., Niculescu, M. C., Purcaru, D. M. (2006). Analysis of PWM converters using MATLAB. International Conference on Simulation, Modelling and Optimization, 22-24 September 2006, Lisbon, 507-512.

Niculescu E., Niculescu M. C., Purcaru, D. M. (2008). Modelling the PWM Zeta converter in discontinuous conduction mode. MELECON 2008 - The 14th IEEE Mediterranean Electrotechnical Conference, Ajaccio, France, 2008, pp. 651-657, doi: 10.1109/MELCON.2008.4618509.

Ogata, K. (2010). Modern Control Engineering (3rd ed., pp. 150-175). New Jersey, Prentice Hall Company.

Peng F. Z., Ridge, O., Lai J.-S., Knoxville. (1997). Multilevel cascaded voltage source inverter with seperate DC source, U.S. Patent 5 642 275, 1–18.

Rahman, M. F., Patterson, D., Cheok, A., Betz, R. (2011). Power Electronics Handbook.

Rodriguez, J., Lai, J-S., Peng, F. Z. (2002). Multilevel inverters: a survey of topologies, controls, and applications, IEEE Transactions on Industrial Electronics, 49, 4, 724–738.

Soomro, J., Memon, D. T., Shah A. M., (2016). Design and analysis of single-phase voltage source inverter using Unipolar and Bipolar pulse width modulation techniques. 2016 International Conference on Advances in Electrical, Electronic and Systems Engineering (ICAEES), Putrajaya, Malaysia, 2016, pp. 277-282, doi: 10.1109/ICAEES.2016.7888052

Viero, R. C., Reis, F. S. (2011). Dynamic modeling of a ZETA converter in DCM applied to low power renewable sources. Energy Conversion Congress and Exposition, 17-22 September 2011, Phoenix, 685-691.

Vuthchhay, E., Bunlaksananusorn, C., Hirata, H. (2008a). Dynamic modeling and control of a zeta converter. International Symposium on Communications and Information Technologies, 21-23 October 2008, Vientiane, 498-503.

Vuthchhay, E., Bunlaksananusorn, C. (2008b). Dynamic modeling of a Zeta converter with State-Space averaging technique. International Conference on Electrical Engineering/Electronics, Computer, Telecommunications and Information Technology, 14-17 May 2008, Krabi, 969-972.

Vuthchhay, E., Bunlaksananusorn, C. (2010). Modeling and control of a Zeta converter. International Power Electronics Conference, 21-24 June 2010, Sapporo, 612-619.

Woranetsuttikul, K., Pinsuntia, K., Jumpasri, N., Nilsakorn, T., Khan-ngern, W. (2014). Comparison on performance between synchronous single-ended primary-inductor converter (SEPIC) and synchronous ZETA converter. International Electrical Engineering Congress, 19-21 March 2014, Chonburi, 1-4.

Wu, B., Narimani, M. (2016). High-power converters and AC drives.

Yılmaz, A., Garip, M. (2017). Tepe akım modu kontrollü Zeta dönüştürücünün küçük işaret analizi. Sakarya Üniversitesi Fen Bilimleri Enstitüsü Dergisi, 21(2): 270-277.

Ziegler, J. G., Nichols, N. B. (1942). Optimum settings for automatic controllers. Transaction fo the ASME, Vol.64, pp. 759–768, 1942.

Zope P., Bhangale, P., Sonare, P., Suralkar, S. (2012). Design and implementation of carrier based sinusoidal PWM inverter. International Journal of advanced research in electrical, electronics and instrumentation engineering, Vol 1, pp. 230-236, October 2012.